Chapter 2
Acoustic Cavitation

Olivier Louisnard and José González-García

1 Introduction

The benefit of acoustic cavitation owes to its ability to concentrate acoustic energy in small volumes. This results in temperatures of thousands of kelvin, pressures of GPa, local accelerations 12 orders of magnitude higher than gravity, shock-waves, and photon emission. In a few words, it converts acoustics into extreme physics.

The counterpart is that it constitutes a complex multidisciplinary problem, involving a wide range of temporal and spatial scales, and is therefore difficult to measure. Furthermore, it is a diphasic problem in essence, with the peculiarity that the cavitation bubbles rise up "from nowhere" and self-arrange in a fascinating variety of structures. For all these reasons it is difficult to control, to predict, and to scale up. Several features of cavitation fields remain unexplained, although the progress in optic recording systems recently shed light on previously unreachable characteristics.

From a theoretical point of view, the physics of the single-bubble model has progressed considerably, thanks to single-bubble sonoluminescence experiments. Many features specific to multibubble fields, however, remain obscure and constitute an active research field. From an engineering point of view, the main unknown remains the bubble size distribution and spatial repartition, which in general constitute the main barrier to extrapolate the more or less known action of one bubble on a specific process, to macroscopically observed effects.

By this contribution, we would like to help the reader to assess the main physics involved when he switches on his sonotrode. This chapter is organized as follows. We first present general results for bubbles in a quiet liquid (Section 2). Then, in Section 3, the purely radial forced oscillations of a single bubble in an infinite liquid will be addressed, focusing on thermal effects, solvent evaporation in inertial

O. Louisnard (✉)
Centre RAPSODEE, FRE CNRS 3213, Université de Toulouse, Ecole des Mines d'Albi, 81013 Albi Cedex 09, France
e-mail: louisnar@enstimac.fr

H. Feng et al. (eds.), *Ultrasound Technologies for Food and Bioprocessing*, Food Engineering Series, DOI 10.1007/978-1-4419-7472-3_2,

bubbles, and their relevance to sonochemistry. Bubbles' loss of sphericity and the resulting effects will be presented in Section 4. The last section addresses cavitation bubble fields and their interaction with the sound field, from both experimental and theoretical points of view.

2 The Quiet Bubble

Before entering in the complex field of acoustic cavitation, it is instructive to examine the behavior of a free spherical gas bubble in a quiet liquid, which can be intuitively apprehended from everyday life.

2.1 A Key Phenomenon: Surface Tension

Increasing the interface between two media requires energy in order to bring molecules from the bulk to the interface. Without a compensating force, an interface therefore has a natural tendency to decrease. In the case of the bubble, the compensating force is an overpressure in the bubble, known as Laplace tension:

$$p_\mathrm{b} = p_0 + \frac{2\sigma}{R} \tag{2.1}$$

where p_0 is the liquid pressure, R is the bubble radius, and σ is the surface tension. This overpressure is unimportant for large bubbles but increases when R approaches the value $2\sigma/p_0$ from above. For example, for an air bubble in water at atmospheric pressure ($\sigma = 0.072$ N^{-1}, $p_0 = 101$ kPa), $2\sigma/p_0$ is 1.45 μm so that the effect of surface tension becomes important in this range of radii. This is precisely the order of magnitude of the bubbles involved in cavitation, so that one can suspect that surface tension will play an important role.

2.2 Bubble Ambient Radius

We consider a bubble containing a given mass m_g of incondensable gas in a liquid at ambient pressure p_0, temperature T_0. The bubble also contains vapor of the liquid, in equilibrium with the latter at T_0, so that the partial pressure of vapor is the equilibrium saturation pressure $p_{\mathrm{v,eq}}(T_0)$. We seek the radius R_0 of such a bubble in mechanical equilibrium. Owing to surface tension, the pressure inside the bubble p_b is $p_0 + 2\sigma/R_0$. Using the law of perfect gases yields

$$p_{\mathrm{v,eq}}(T_0) + \frac{m_\mathrm{g}}{M_\mathrm{g}} \frac{\mathcal{R}T_0}{\frac{4}{3}\pi R_0^3} - \frac{2\sigma}{R_0} = p_0 \tag{2.2}$$

This cubic equation yields the bubble ambient radius R_0. The vapor pressure $p_{v,eq}(T_0)$ can be neglected for temperature well below the boiling point. For further use, we define the dimensionless Laplace tension for the bubble in ambient conditions

$$\alpha_S = \frac{2\sigma}{p_0 R_0} \tag{2.3}$$

2.3 Radial Mechanical Stability: The Blake Threshold

Equation (2.2) gives the radius of a bubble in mechanical equilibrium for a given liquid ambient pressure p_0. One might look for the evolution of the bubble radius from R_0 to R when the liquid pressure p_0 is decreased to $p = p_0 - p_a$. Assuming that this variation is slow enough to allow isothermal transformations of the gas, the evolution of R can be obtained implicitly by

$$p_{v,eq}(T_0) + \left(p_0 - p_{v,eq}(T_0) + \frac{2\sigma}{R_0}\right)\left(\frac{R_0}{R}\right)^3 - \frac{2\sigma}{R} = p_0 - p_a \tag{2.4}$$

Rather than seeking explicitly R from Equation (2.4), it is more instructive to look for a graphical solution. Figure 2.1 is obtained by using Equation (2.4), and it shows the variation of the equilibrium radius R as a function of the liquid pressure $p_0 - p_a$. It is seen that if the external pressure is lowered to a value smaller than $p_0 - p_a^{crit}$, there is no possible equilibrium radius R. Physically, at this point, the liquid starts to flow outward and the bubble undergoes an explosive expansion. This analysis is the key point of inertial cavitation.

This critical value p_a^{crit}, which depends on R_0 and thus on the quantity of gas m_g contained in the bubble, is called the "Blake threshold" (Akhatov et al., 1997a; Blake, 1949; Hilgenfeldt et al., 1998; Louisnard and Gomez, 2003) and can be calculated explicitly by seeking the minimal value of R from Equation (2.4). This yields

$$p_a^{crit} = p_0 - p_{v,eq} + p_0 \left(\frac{4}{27}\frac{\alpha_S^3}{1+\alpha_S}\right)^{1/2} \tag{2.5}$$

The values of p_a^{crit} are represented in Fig. 2.2 for an air bubble in water in ambient conditions ($\sigma = 0.0725\ \mathrm{N \cdot m^{-1}}, p_{v,eq} = 2,000\ \mathrm{Pa}, p_0 = 100\ \mathrm{kPa}$).

An important point to note from Equation (2.5) and Fig. 2.1 is that the corresponding external pressure $p_0 - p_a^{crit}$ can be lower than the vapor pressure of the liquid, and even negative for small values of R_0. It should be recalled that a liquid, owing to internal cohesion force, can effectively support negative pressures or "tensions" (see Section 5.2).

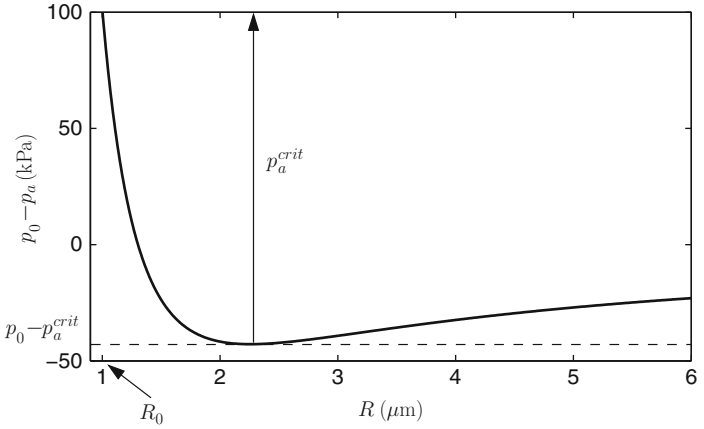

Fig. 2.1 Evolution of the bubble equilibrium radius R when the liquid pressure $p_0 - p_a$ is decreased, for a 1-μm bubble in ambient conditions

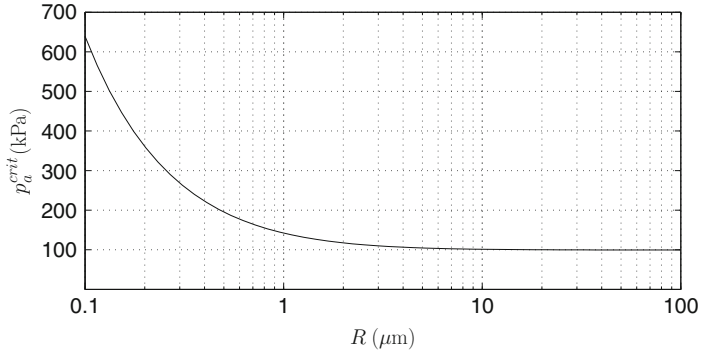

Fig. 2.2 Blake threshold for an air bubble in water in ambient conditions ($p_0 = 101325$ Pa, $\sigma = 0.0725\ \mathrm{N \cdot m^{-1}}$)

2.4 Perturbations of Radial Equilibrium: Free Frequency

The gas filling the bubble provides elasticity to the bubble/water mechanical system; the bubble will oppose a resistance to any compression or expansion imposed by the liquid motion. This force may in turn put the liquid into motion, so that the bubble/liquid constitutes a mass–spring system. Perturbing the bubble slightly from its equilibrium radius therefore results in free radial oscillations, whose frequency can be calculated from energy conservation consideration or from a bubble dynamics equation (see Section 3.2.3). If the oscillations are assumed isothermal, the angular frequency of the free oscillations reads

$$\omega_0 = \frac{1}{R_0}\left\{\frac{p_0}{\rho_1}\left[3(1+\alpha_S)-\alpha_S\right]\right\}^{1/2} \tag{2.6}$$

where ρ_1 is the liquid density.

Bubble-free oscillations are responsible for the noise emitted by running water. In the context of acoustic cavitation, one would expect that a bubble excited at its free frequency would undergo strong oscillations and would be the main factor for cavitation effects. Active bubbles in strong sound fields are in fact excited well below their resonant frequency, as will be discussed throughout further in the chapter.

2.5 Gas Exchange with the Liquid

In saturation condition, that is, if the liquid is saturated with gas at ambient pressure p_0, a gas bubble dissolves because of surface tension. This can be readily understood from Fick's law, as shown below.

Let us denote C_∞ as the concentration of dissolved gas in the solution, and let us consider a bubble of ambient radius R_0 in mechanical equilibrium in the liquid. Far from the bubble, the concentration is C_∞. At the bubble wall, the dissolved gas is in equilibrium with the gas inside the bubble, at pressure $p_{g_0} = p_0 + 2\sigma/R_0$ (let us neglect vapor to simplify the reasoning). Therefore, by virtue of Henry's law, the dissolved gas concentration at the bubble wall is $C_R = p_{g_0}/k_g$, where k_g is the Henry constant. We therefore express the difference in concentration between the bubble wall and at infinity as

$$C_R - C_\infty = C_0\left[\frac{p_{g_0}}{p_0} - \frac{C_\infty}{C_0}\right] = C_0\left[1+\alpha_S - \frac{C_\infty}{C_0}\right] \tag{2.7}$$

where $C_0 = p_0/k_g$ is the saturation concentration, that is the concentration of dissolved gas in the liquid in equilibrium with the gas at p_0. Thus if $C_\infty/C_0 < 1$ the liquid is under-saturated, if $C_\infty/C_0 > 1$ the liquid is supersaturated (as is the case in bubbly beverages that are saturated in CO_2 at a few bars)

For a saturated liquid, we have $C_\infty/C_0 = 1$, so that from Equation (2.7), $C_R - C_\infty > 0$. Fick's law thus predicts an outward gas diffusion flux, so that the bubble dissolves increasingly faster as its size decreases. The analytical solution of the problem has been given by Epstein and Plesset (1950). A practical implication of this phenomenon is that no stable gas bubble should exist in a quiet saturated liquid.

If the liquid is supersaturated in gas, that is $C_\infty/C_0 > 1$, Equation (2.7) shows that there exists a critical value of R_0 above which the bubble grows by gaining gas from the liquid, and below which it dissolves. The bubble growth can be easily observed in a glass of champagne, for example.

In a sound field, an oscillating bubble can grow even in a saturated or under-saturated liquid. The phenomenon is termed "rectified diffusion" and will be discussed in Section 3.4.

2.6 Translational Motion

Common observation tells us that a bubble rises. This is because the buoyancy force $\mathbf{F_A} = -4/3\pi R_0^3 \rho_l \mathbf{g}$ is greater in magnitude than the weight of the bubble $\mathbf{F_G} = 4/3\pi R_0^3 \rho_b \mathbf{g}$, where ρ_b is the bubble density. After some time, the bubble will reach a steady velocity, which can be obtained by balancing the buoyancy force $\mathbf{F}_\mathrm{A}$ with the viscous drag force $\mathbf{F_V} = -4\pi R_0 \mu_l \mathbf{v}$ (the weight being negligible since $\rho_\mathrm{b} \ll \rho_\mathrm{l}$):

$$\mathbf{v} = -\frac{1}{3} R_0^2 \frac{\rho_\mathrm{l}}{\mu_l} \mathbf{g}$$

where μ_l is the dynamic viscosity of the liquid.

In a sound field a bubble undergoes generalized buoyancy forces, termed Bjerknes forces, and can be either attracted or repelled by zones of high acoustic pressures. They also undergo mutual attraction or repulsion as they experience the field radiated by a neighboring bubble. This issue will be presented in Section 5.3.

2.7 Departure from Spherical Shape

Above some critical size, quiet bubbles depart from their spherical shape as they rise in the liquid, generally flattening their rear part. Radially oscillating bubbles exhibit various shape instabilities, leading to their destruction, and have a peculiar behavior near solid boundaries (Section 4).

3 The Forced Spherical Single Bubble

3.1 Introduction

This section recalls the main features of a radially oscillating spherical bubble in an infinite liquid. This ideal picture may sound unrealistic, and anyone having looked at a cavitation experiment may have doubts on its practical use. However, it leads to important fundamental results, whose usefulness in cavitation prediction has been proved. Moreover, levitation experiments of single bubbles, designed much earlier than their initial use by Gaitan et al. (1992) for single-bubble sonoluminescence (SBSL), produced numerous experimental confirmations of theory in a configuration relevant to the above hypothesis.

This section will refer frequently to recent theoretical and experimental work developed in the context of SBSL. This is because the latter issue has raised numerous papers presenting either new issues or theoretical and experimental refinements of known results. Most of these results are also relevant to multibubble fields.

In this section, after presenting the equations governing the forced oscillations of a spherical bubble and their reduction in the linear case, we will focus on the

case of inertial oscillations, which is responsible for most of the practical effects of acoustic cavitation. The thermal behavior of the bubble interior, along with vapor and gas transport at the interface will next be discussed. The chemistry in the bubble will only be briefly mentioned, and we refer the reader to the chapter of K.S. Suslick in this book. Finally, the rectified diffusion phenomenon, possibly leading to accumulation of gas in the bubble, will be presented.

3.2 Radial Oscillations

3.2.1 Rayleigh–Plesset Equations

Rayleigh (1917) studied the collapse of a spherical empty cavity, whatever its origin, in order to assess its possible responsibility for the erosion damage on ship propellers. He derived a differential equation, which is basically the principle of mechanical energy conservation in the absence of dissipative forces.

We assume a spherical bubble filled with incondensable gas and vapor, in a liquid of infinite extent, and we first neglect gas transport between the liquid and the bubble. A correct representation of the problem would require the resolution of conservation equations in both phases, but several levels of approximations have allowed us to obtain the equation of motion in the form of a second-order ordinary differential equation.

The most common assumption is the uniformity of the pressure inside the bubble, which, along with the liquid incompressibility hypothesis, yields the Rayleigh–Plesset family of equations (Noltingk and Neppiras, 1950; Plesset, 1949). The first assumption is questionable in view of the order of magnitude of the bubble wall velocities, which may attain several times the sound velocity in the gas. The validity of this assumption has been addressed recently by Lin et al. (2002a), and the Rayleigh–Plesset equation, almost one century after its first derivation, was finally found to be valid in a very wide range of parameters. In its most basic form, it reads

$$R\ddot{R} + \frac{3}{2}\dot{R}^2 = \frac{1}{\rho_\mathrm{l}}\left[p_\mathrm{b}(t) - \frac{2\sigma}{R} - 4\mu_\mathrm{l}\frac{\dot{R}}{R} - p(t)\right] \tag{2.8}$$

where over-dots denote time derivatives. $p(t)$ is the driving pressure, which can be understood as either the pressure infinitely far from the bubble, or the pressure that would be measured in the liquid at the bubble center, if the latter would be absent. For sinusoidal driving, $p(t)$ can be written as

$$p(t) = p_0 - p_\mathrm{a} sin(\omega t) \tag{2.9}$$

where p_a is the driving pressure amplitude, and ω is the angular frequency of the driving. In what follows, we note $f = \omega/2\pi$ the frequency, and $T = 1/f$ the period of the driving. It should be noted that a value of p_a greater than p_0 means that the liquid pressure becomes negative during some part of the expansion phase.

The pressure p_b in the bubble is the sum of the partial pressures of gas p_g and vapor p_v. We neglect vapor for now and will detail this issue in Section 3.3.5. Expression of the uniform pressure in the bubble $p_g(t)$ depends on the thermal behavior of the gas and the equation of state chosen. The gas may be considered as perfect, except at the end of the collapse, where it reaches high density so that van der Waals repulsion forces between atoms or molecules become important. Keeping the assumption of perfect gas, the gas pressure may be written as $p_{\mathrm{g}_0}(R_0/R)^3$ in the isothermal limit, and $p_{\mathrm{g}_0}(R_0/R)^{3\gamma}$, in the adiabatic limit, where γ is the ratio of the gas specific heats. A more detailed analysis of thermal effects shows that, in fact, none of these assumptions is uniformly valid, and we will detail this point in Section 3.3.

3.2.2 Effects of Liquid Compressibility

The compressibility of a medium can be neglected when the typical length of the system (the bubble radius R) is much lower than the wavelength. The latter is $c_\mathrm{l}\tau_\mathrm{dyn}$, where τ_dyn is the characteristic timescale of the bubble oscillation, and c_l the sound speed in the fluid.

For linear oscillations, τ_dyn is simply the acoustic period $1/f$ and $R \simeq R_0$, so that the conditions reads $R_0 \ll c_\mathrm{l}/f$. Compressibility can therefore be neglected for low frequency, and one may expect compressibility effects for high frequencies. This is indeed the case and is one of the reasons for damping of the oscillations (see Section 3.2.3).

For arbitrary oscillations, $\tau_\mathrm{dyn} \simeq R/\dot{R}$ so that compressibility can be neglected if $\dot{R} \ll c_\mathrm{l}$. This is not fulfilled for inertial cavitation, where the bubble wall can attain c_l or even more. Corrections to the Rayleigh equation thus involve corrective terms in $\dot{R}/c_\mathrm{l}$. Several compressible equations have been derived over the years (see Lezzi and Prosperetti, 1987; Prosperetti, 1999; Prosperetti and Lezzi, 1986, and references herein), and it has long been discussed to assess which form was the most appropriate, up to the work of Prosperetti and Lezzi (1986; Lezzi and Prosperetti, 1987) who rigorously derived classes of equations of first and second order. Their formulation recovers many earlier results, among which is the Keller equation (Keller and Miksis, 1980)

$$R\ddot{R}\left(1-\frac{\dot{R}}{c_\mathrm{l}}\right)+\frac{3}{2}\dot{R}^2\left(1-\frac{\dot{R}}{3c_\mathrm{l}}\right)= \frac{1}{\rho_\mathrm{l}}\left[\left(1+\frac{\dot{R}}{c_\mathrm{l}}+\frac{R}{c_\mathrm{l}}\frac{\mathrm{d}}{\mathrm{d}t}\right)\left(p_\mathrm{g}-p(t)\right)-\frac{2\sigma}{R}-4\mu_\mathrm{l}\frac{\dot{R}}{R}\right] \tag{2.10}$$

3.2.3 Linear Oscillations

The radial oscillations of a bubble are in essence non-linear. This can be seen mathematically from Equation (2.10), but can be more easily understood from a physical point of view (Lauterborn and Mettin, 1999): a bubble can be expanded to an

arbitrary size, but can be compressed only down to near zero radius. However, if one considers only low amplitude driving pressure, the bubble can respond with small oscillations around its ambient radius R_0. In this range, the bubble/water system can be considered as a linear forced oscillator, similar to a mass–spring system excited by a periodic force. Mathematically, this approximation can be easily obtained by setting

$$p(t) = p_0[1 + P\mathrm{e}^{\mathrm{i}\omega t}], \qquad R(t) = R_0\left[1 + X\mathrm{e}^{\mathrm{i}\omega t}\right] \tag{2.11}$$

in Equation (2.10) and neglecting terms of order greater than 1 in X or P. A linear relation is then obtained between the complex amplitudes of the bubble radius X and of the driving P:

$$X = \frac{1}{\rho_1 R_0^2}\,\frac{1}{\omega_0^2 - \omega^2 + 2\mathrm{i}b\omega}\,P \tag{2.12}$$

with

$$\omega_0 = \frac{1}{R_0}\left\{\frac{p_0}{\rho_1}\left[3\eta(1+\alpha_S) - \alpha_S\right]\right\}^{1/2} \tag{2.13}$$

$$2b = \frac{4\mu_1}{\rho_1 R_0^2} + \frac{\omega^2 R_0}{c_1} + \frac{p_0(1+\alpha_S)}{\rho_1 \omega R_0^2}\Im\Phi \tag{2.14}$$

where η is either 1 for isothermal, or γ for adiabatic behavior of the gas, respectively. More generally, η may take intermediate values, known as polytropic exponent, representing in an approximate way the diffusive heat transport between the bubble and the liquid (see Section 3.3). The damping factor b is the sum of three contributions: the first is due to viscous dissipation in the liquid, the second corresponds to energy loss by acoustic radiation in the compressible fluid, and the last owes to energy dissipation by heat diffusion in the gas ($\Im$ denotes the imaginary part of a complex number, and the value of Φ can be found in Prosperetti, 1977a).

From Equation (2.12), we can recover expected results for the bubble as a forced harmonic oscillator, which we think is important to review here:

- for $\omega < \omega_0$, the bubble radius is out of phase with the driving pressure (if we neglect the term $2\mathrm{i}b$). Thus, the bubble expands in the depression phase of the driving, which is the intuitively expected behavior.
- for $\omega > \omega_0$, the bubble radius is in phase with the driving pressure. This may sound intriguing since in that case, the bubble expands as the external pressure increases. This owes to the predominance of liquid inertia at high frequencies. It has practical consequences on the direction of the Bjerknes force (Section 5.3.1), or the acoustic opacity of bubbly liquids to waves of frequency larger than the bubble's resonance frequency (see Section 5.1.4).

- the bubble oscillations become increasingly large for frequencies near ω_0. It should be noted that such large amplitudes may invalidate the basic hypothesis on the weakness of the oscillations.

Acoustic cavitation is generally far from the linear regime, but the above remarks can help to understand some basic features. However, they predict wrong results at high drivings, especially for Bjerknes forces (Section 5.3.1).

Experimentally, the driving frequency $f = \omega/2\pi$ is a fixed parameter, while all bubbles ambient sizes may a priori exist in the liquid. It is therefore useful to define the resonance radius $R_{\rm res}$, which is the radius that a bubble should have to be resonant at ω. It can be obtained from Equation (2.13), replacing ω_0 by ω and R_0 by R_r. Neglecting surface tension terms ($\alpha_S \ll 1$), and assuming isothermal oscillations, we get

$$R_{\rm res} = \frac{1}{2\pi f}\left(\frac{3p_0}{\rho_{\rm l}}\right)^{1/2} \tag{2.15}$$

In the case of a bubble in water in ambient conditions, we may retain the approximate relation $R_{\rm res} f = 3\ {\rm m}\cdot{\rm s}^{-1}$. For $f = 20$ kHz, the resonant radius is 150 μm, while for $f = 1$ MHz, it drops down to 3 μm.

3.2.4 Non-linear Oscillations

When excited at larger amplitudes, the bubble oscillations can exhibit a rich collection of non-linear phenomena. To get a rapid insight into these behaviors, it is convenient to vary one or several parameters (among R_0, $p_{\rm a}$, and f) and to display only the maximum radius attained by the bubble over one cycle for this parameter. The curves obtained are termed "response curves." A large collection of such curves can be found in Lauterborn and Mettin (1999). We summarize these results below.

Non-linear resonances: When the ratio of the linear resonance frequency and the driving frequency f_0/f (or equivalently the ratio of the resonant radius to the ambient radius $R_{\rm r}/R_0$) approaches a rational number n/m, a non-linear resonance can occur and the amplitude of the bubble oscillations increases. This can be seen in the small peaks in the lower curve of Fig. 2.3. The 1/1 peak corresponds to the linear resonance frequency. Following the accepted terminology, the resonances $n/1$ are called harmonic resonance, the resonances $1/m$ are sub-harmonic resonances, while rational ratio n/m resonances are ultra-harmonic resonances (Lauterborn, 1976).

Period doubling and chaos: Period doubling denotes the destabilization of a non-linear oscillator, when varying one parameter (here R_0), to oscillations with a period twice as large as the driving. In this case two different maxima would be recorded, the first on even driving periods, the second on odd ones. This can be visualized by a separation of the response curve in two branches (see upper curve in Fig. 2.3 near $R_0 = 45$ μm). Changing the parameter yields further destabilizations toward period-4, period-8, and so on, ending in a chaotic regime. The latter is aperiodic and a different maximum is recorded at each driving period. This yields the clouds of

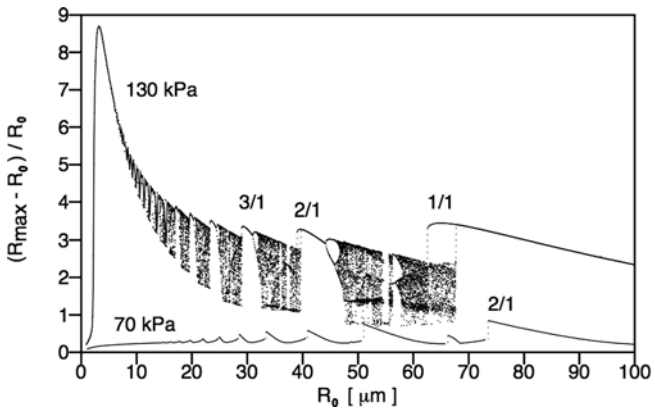

Fig. 2.3 Response curves for an air bubble driven at $f = 20$ kHz (the resonance radius is about 150 µm in this case), $p_a = 70$ kPa (*lower curve*), and $p_a = 130$ kPa (*upper curve*) as a function of the bubble ambient radius. The *fractional numbers* indicate the order of the resonances. Adapted from Sonochemistry and Sonoluminescence (1999, pp. 63–72), in the chapter "Nonlinear Bubble Dynamics: Response Curves and More" by Lauterborn and Mettin. With kind permission of Springer Science and Business Media

dots in the upper curve of Fig. 2.3 (period-4 and higher are scarcely visible because they occur in a narrow parameter range). These successive transitions are termed "sub-harmonic route to chaos."

The experimental consequence of period doubling is the appearance of a spectral component at *f*/2 in the emitted cavitation noise (Neppiras, 1969). The route to chaos has furthermore been demonstrated experimentally by Lauterborn and Cramer (1981a, b), who recorded *f*/2, *f*/4 spectral components, and finally broadband noise, as the driving was increased. The appearance of either a sub-harmonic spectral component *f*/2, or a broadband spectrum, is generally considered as a mark of strong cavitation, and has been correlated experimentally to erosive effects (Gaete-Garreton et al., 1997).

3.2.5 Dynamical Blake Threshold

A noticeable change can be observed between the two curves of Fig. 2.3 in the range [0, 10] µm. At 70 kPa, the response curve is monotonic, while at 130 kPa, the curve passes to a very marked maximum. This peak is termed "giant resonance" by Akhatov et al. (1997a), and is much larger than the main resonance 1/1. This feature has important implications for many cavitation phenomena, especially for diffusional stability of bubbles in levitation cells (Section 3.4.3), and inversion of Bjerknes forces (Section 5.3.1).

A zoom on the small range of R_0 can be seen in Fig. 2.4, for 130 kPa and higher drivings. It is seen that, starting from small radii, the response curves increase suddenly for a driving-dependent critical value of R_0. If conversely, p_a were increased

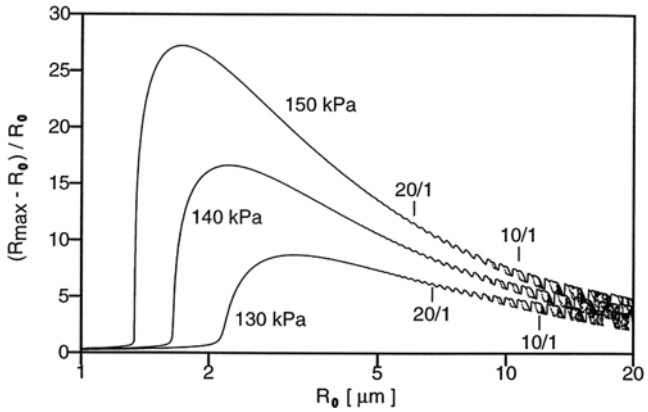

Fig. 2.4 Same as Fig. 2.3 in a range of smaller R_0 and large drivings. Adapted from Sonochemistry and Sonoluminescence (1999, pp. 63–72), in the chapter "Nonlinear Bubble Dynamics: Response Curves and More" by Lauterborn and Mettin. With kind permission of Springer Science and Business Media

for constant R_0, a similar brutal transition would be found (somewhere between the two curves of Fig. 2.3).

This is exemplified in Fig. 2.5, which represents one period of oscillation of a 1 μm bubble for three very close value of the driving p_a near 143 kPa, simulated

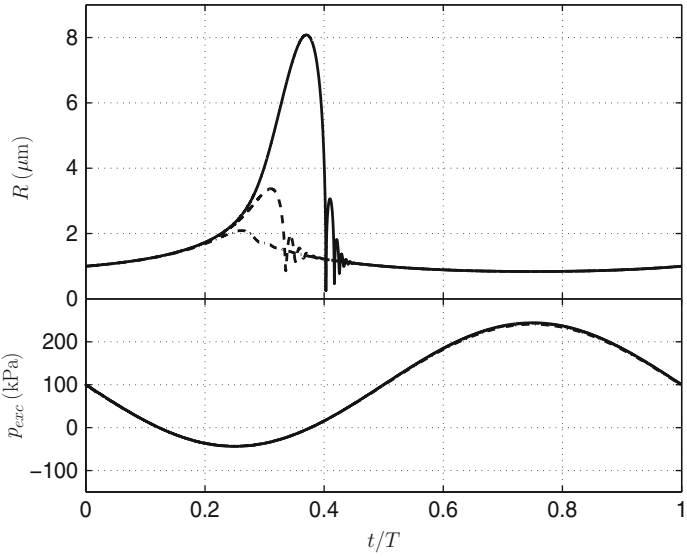

Fig. 2.5 *Upper graph*: dynamics of a 1-μm bubble driven at $f = 20$ kHz, driving amplitudes $p_a = 142$ kPa (*dash-dotted line*), 143.5 kPa (*dashed line*), and 144 kPa (*solid line*). The transition from stable to inertial oscillations can be clearly identified. *Lower graph*: corresponding driving pressures. The three curves are indistinguishable

from Equation (2.10). The bubble dynamics switches drastically from quasi-static oscillations (dash-dotted curve) to large amplitude ones. It is interesting to note that the three curves are indistinguishable at the beginning of the cycle, up to t slightly above $0.2T$.

In fact, this transition occurs at the Blake threshold, calculated from static arguments in Section 2.3. Its physical origin is a competition between the explosive motion caused by the liquid negative pressures and the stabilizing effect of surface tension (Akhatov et al., 1997a; Hilgenfeldt et al., 1998; Lauterborn and Mettin, 1999; Louisnard and Gomez, 2003). For the lowest driving, surface tension prevents the bubble to expand, while it can no longer do so for the largest. For a fixed p_a, Equation (2.5) can be inverted to yield a critical radius R_0^{crit}, which would coincide with the lift-off of the response curves in Fig. 2.4.

3.2.6 Inertial Oscillations

The upper curve in Fig. 2.5 displays an explosive growth, stopped by the recompression of the driving. The growth is then followed by a rapid collapse because the low internal pressure in the bubble at its maximum radius cannot retain the liquid to flow inward. This is the characteristic of "inertial oscillations." The term "inertial" refers to the large explosive expansion of the bubble ($0.25 < t/T < 0.35$ in the upper curve of Fig. 2.5), during which the motion is mainly governed by the liquid inertia. Inertial bubbles have been termed "transient bubbles" in the past, since at that time many experimental observations evidenced bubbles undergoing fragmentation after collapse (see Section 4). The SBSL experiments demonstrate that this is not necessarily the case, and SBSL bubbles are a typical example of inertial and stable bubbles.

Inertial oscillations appear in the parameter space just above the Blake threshold, and are in fact the only bubbles present in the high-pressure zone of strong sound fields (see Section 5.4.5). Inertial bubbles are the main contributors for most applications, owing to the extreme conditions mentioned hereafter.

3.2.7 The Bubble Collapse

We now turn to a brief description of the bubble collapse. The potential energy stored during expansion is then converted into kinetic energy of the liquid and the inward velocity increases drastically, possibly exceeding the sound velocity in the liquid. This is the original problem treated analytically by Rayleigh (1917), who derived scaling laws for the radius versus time (see also Hilgenfeldt et al., 1998; Löfstedt et al., 1993).

The collapse is stopped by the compression of incondensable gas in the bubble. The gas density increases and the van der Waals repulsion forces between molecules or atoms prevent further compression. The bubble rebounds on a timescale of the order of a few nanoseconds. The end of the collapse is almost adiabatic (see Section 3.3.4), and the gas is heated up to thousands of Kelvin, which can promote chemical reactions and sonoluminescence. The bubble internal pressure may

increase up to 1 GPa or more, and the outward acceleration as the bubble rebounds may reach 10^{12} g. The short timescale involved can reveal the effect of the compressibility of the liquid. A diverging spherical wave is emitted, which causes energy loss by radiation (Hilgenfeldt et al., 1998). This wave may steepen into a shock, whose characteristics have been calculated by Benjamin (1958), Tomita and Shima (1977), and Fujikawa and Akamatsu (1980) and demonstrated experimentally by Pecha and Gompf (2000). Shockwaves emitted from collapsing bubbles are held responsible for particle desagglomeration and emulsification (Li and Fogler, 2004).

After the rebound, the bubble expands again and undergoes secondary collapses, termed "afterbounces." The decay of these afterbounces is closely linked to the energy loss in the primary collapse, which in turn depends on several parameters: quantity of solvent in the bubble, thermal diffusion, and chemical reactions among others. The frequency of these rebounds is more or less the free frequency of the bubble. Indeed, the collapse acts mainly as an impulse excitation on a nearly free bubble, to which the latter responds with oscillations at its Eigen-frequency. These afterbounces play an important role in the spherical stability of bubbles (see Section 4).

Let us note that the energy restored in the collapse, in any form, is the potential energy stored during expansion. The latter decreases with frequency, since the bubble has less time to expand. One therefore expects less intense collapses as frequency increases, but this competes with the higher number of collapses per unit time. At the scale of a single bubble, some effects may therefore exhibit an optimum as frequency varies. A generalization for multibubble configuration is difficult because frequency also has effects on the acoustic field and the bubble size distribution. However, such effects have been observed in sonochemistry (see for example Pétrier and Francony, 1997).

3.3 Thermal Effects in the Bubble

3.3.1 The Physics

When the bubble is compressed, the gas in the bubble is heated. Because the surrounding liquid is colder, heat can escape by diffusion from the bubble toward the liquid. The center of the bubble is therefore hotter than the surface, and the opposite holds during the bubble expansion. Hence, the gas is not in thermal equilibrium and, rigorously, its behavior is neither isothermal nor adiabatic. Furthermore, the existence of temperature gradients implies an irreversible loss of energy over one oscillation cycle.

One may first wonder if temperature gradients also exist in the liquid. During bubble compression, for example, does this outward heat flux increase noticeably the temperature of the liquid near the bubble surface? This is an important issue for applications of cavitation, since the liquid may contain non-volatile species that may be altered by high temperatures (chemical reactions for sonochemistry or phase transition for sonocrystallization). A rough estimate of the liquid temperature increase

near the bubble surface can be obtained by using the continuity of the heat flux at the bubble (Prosperetti et al., 1988):

$$\frac{T_R - T_0}{T_C - T_R} = \left(\frac{K_g C_{p_g} \rho_g}{K_l C_{p_l} \rho_l} \right)^{1/2} \tag{2.16}$$

where T_R is the temperature of the liquid at the bubble surface, T_C is the temperature at the bubble center, and T_0 is the undisturbed liquid temperature far from the bubble. K, C_p, and ρ are the thermal conductivities, specific heats, and densities of the gas (subscript g), and of the liquid (subscript l), respectively. The right-hand side being typically of the order of 10^{-3} to 10^{-2}, the temperature variations of the liquid near the bubble surface are expected to be two or three orders of magnitude smaller than the ones at the bubble center.

The calculation of the gas pressure in the bubble (p_g in Equation (2.10)) requires the knowledge of the temperature field. The isothermal and adiabatic approximations avoid this difficulty, but should be considered as extreme ideal cases. The real behavior is governed by the equation of energy conservation in the gas phase (Prosperetti, 1991; Prosperetti et al., 1988), but it is instructive to draw a general picture from the comparison of the timescale of bubble dynamics τ_{dyn}, and the diffusive timescale τ_{diff}, whose ratio is the Peclet number Pe.

3.3.2 Linear Oscillations

For linear oscillations, $\tau_{dyn} = 1/f$ and $\tau_{diff} = R_0^2/\chi_g$, where $\chi_g = K_g/\rho_g C_{p_g}$ is the diffusivity of the gas, so that the thermal Peclet number is $\mathrm{Pe}_0 = \tau_{diff}/\tau_{dyn} = R_0^2 f/\chi_g$. A small value of Pe_0 (for a low frequency, or small bubbles) means that the diffusive timescale is very small, so that the gas will equilibrate immediately in response to a compressional heating and the bubble behaves isothermally. Conversely, for a large value (for high frequency, or large bubbles), heat cannot escape from the bubble, and the gas behaves adiabatically. For intermediate values, temperature gradients exist in the bubble interior, and part of the compressional heating can escape from the bubble.

The resolution of the problem within the linear approximation yields the gas pressure as a linearized form of

$$p_g = p_{g_0} \left(\frac{R_0}{R} \right)^{3\eta} \tag{2.17}$$

where η is called "polytropic exponent" (Devin, 1959; Prosperetti, 1977a) and can be expressed as a function of Pe_0. The limit cases η=1 for $\mathrm{Pe}_0 \to 0$, and η=γ for $\mathrm{Pe}_0 \to \infty$, are recovered in the isothermal and adiabatic limits, respectively. It should be noted that thermal diffusion also introduces a net energy loss over one period, contributing to the damping of the oscillations (see the third term in Equation (2.14)).

3.3.3 Non-linear Oscillations

The above simplified picture is satisfactory for linear or weakly non-linear oscillations, and far from resonances, and in agreement with experimental results (Crum, 1983; Crum and Prosperetti, 1983). It is known to fail, however, near resonances (see the discussion in Crum and Prosperetti, 1984).

For non-linear oscillations, a correct treatment of thermal diffusion in the bubble requires the resolution of the energy conservation equation in the gas. Approximate analytical solutions were proposed by Miksis and Ting (1984), Prosperetti (1991), and Kamath et al. (1992). Several numerical schemes have also been developed (Kamath and Prosperetti, 1989; Kamath et al., 1993; Prosperetti et al., 1988) and were shown to modify the response curves, especially near resonances, but were restricted to moderate drivings.

3.3.4 Inertial Bubbles

The maximum temperature obtained at the end of a perfect spherical collapse is a crucial issue for sonoluminescence and sonochemistry.

The main characteristic of inertial cavitation is the short timescale of the collapse, which may be much shorter than the diffusion timescale. Thus, during the final part of the collapse, the gas is expected to behave almost adiabatically. This idea was followed in the early paper of Noltingk and Neppiras (1950) in order to estimate the final collapse temperature:

$$T(R_{\min}) = T_0 \left(\frac{R_i}{R_{\min}} \right)^{3(\gamma-1)} \tag{2.18}$$

where R_i is the radius from which the behavior starts to be adiabatic. Noltingk and Neppiras (1950) considered the transition to occur at maximum radius. This result already indicated that in otherwise similar conditions, higher temperatures should be obtained for higher values of γ, so that a collapsing mono-atomic gas bubble is hotter than a polyatomic gas bubble (air for example). This is why sonochemical yields can be enhanced by bubbling the solution with argon or other noble gases. The decrease of multibubble sonoluminescence intensity when adding a small propane fraction in argon is a clear experimental demonstration of this effect (McNamara et al., 1999).

The timescale of the bubble expansion is three or four orders of magnitudes larger than that of the collapse, and can be much larger than the diffusive timescale, so that the bubble expansion and the initial stage of the collapse can be isothermal, the final stage being adiabatic. Hence, no two approximations are uniformly appropriate. In fact, the behavior of the gas in the different parts of the bubble oscillation now depends on the instantaneous value of the Peclet number $\mathrm{Pe}(t) = \tau_{\mathrm{diff}}/\tau_{\mathrm{dyn}}$, where $\tau_{\mathrm{diff}} = R(t)^2/\chi_{\mathrm{g}}$ and $\tau_{\mathrm{dyn}} = R(t)/|\dot{R}(t)|$. It is therefore tempting to extend the linear results by defining a dynamic polytropic exponent from $\mathrm{Pe}(t)$, so that the gas behavior automatically varies between isothermal and adiabatic. This approach

was used by Hilgenfeldt et al. (1999b) and independently by Storey and Szeri (2001), and were used successfully within a self-consistent theory of single-bubble sonoluminescence (Hilgenfeldt et al., 1999a, b).

A refined approach accounting for thermal (and also mass) diffusion, using a dynamic thermal diffusion length has been proposed by (Brenner et al., 2002; Toegel et al., 2000a), and found to be in good agreement with direct Navier–Stokes calculations of Storey and Szeri (2000). Yasui (1997) proposed a similar model independently. During compression, part of the compressional heat escapes toward the liquid by thermal diffusion, and therefore, the lower the thermal conductivity of the gas, the hotter the temperature reached in the bubble. This suggested that for noble gas bubbles, the collapse temperature should increase in the series He, Ne, Ar, Kr, Xe. This is indeed the case and is demonstrated unambiguously by the experimental results of Didenko et al. (2000) for multibubble cavitation.

3.3.5 Solvent Evaporation and Condensation

When the bubble expands, the internal pressure decreases, so that the volatile species must evaporate into the bubble to restore equilibrium. Conversely, when the bubble shrinks, condensation takes place. Therefore, if there is equilibrium at the bubble surface, accounting for the presence of vapor can be done easily by setting the partial vapor pressure p_v in the bubble to $p_{v,eq}$, the number of molecules of solvent adjusting to the bubble volume variations.

However, in view of the very short timescale of the bubble collapse, two processes limit this mass transport. First, evaporation and condensation have finite kinetics, so that the vapor in the bubble may not have enough time to condense during the collapse. Secondly, the vapor is not alone in the bubble and its diffusive transport through other species (typically air or any incondensable gas) can be limited. Storey and Szeri (2000) considered both phenomena in their model and found that the water transport in sonoluminescing bubbles was mainly diffusion-limited.

As seen above, the final temperature of the adiabatic collapse is very dependent on γ. Any solvent vapor present in the bubble lowers γ and therefore the final bubble temperature. It is therefore expected that the presence of a volatile species in the liquid will cool the bubble content. This is evidenced by experiments on SBSL intensity in water contaminated with various alcohols (Ashokkumar et al., 2000, 2002; Toegel et al., 2000b). Similarly, lowering the temperature decreases the vapor pressure, lowers the solvent evaporation into the bubble, and should thus increase the collapse temperature. This is confirmed by the experiments of McNamara et al. (1999) in octanol at various bulk temperatures. The higher brightness of SBSL in cold water (Barber et al., 1994; Hiller et al., 1992; Vazquez and Putterman, 2000) is also attributed to this effect (Storey and Szeri, 2000, 2002; Toegel et al., 2000a; Vazquez and Putterman, 2000; Yasui, 2001).

The effect of vapor pressure is exemplified in Fig. 2.6, obtained by using the model of Toegel et al. (2000a) for a 4 μm argon bubble in water at 25°C (solid lines) and 1°C (dashed lines), driven at 120 kPa, 26,500 Hz. The upper graph represents the radius-time curves. The bubble expands less in cold water because less vapor

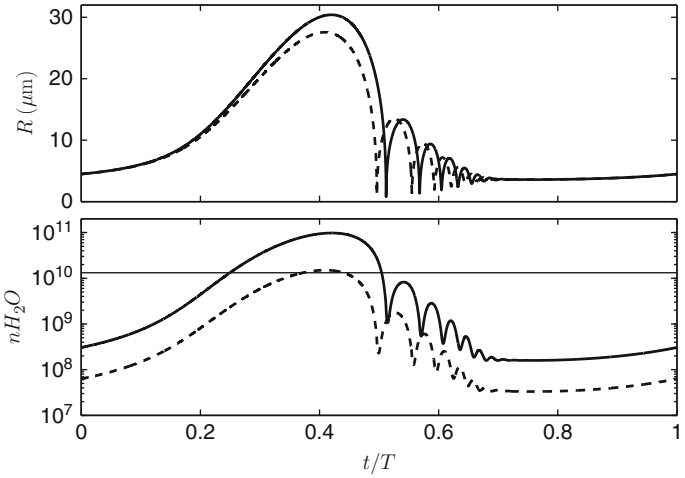

Fig. 2.6 Radius-time curves (*upper graph*) and number of water molecules in the bubble (*lower graph*) for a 4-μm Argon bubble in water at 25°C (*solid lines*) and 1°C (*dashed lines*), driven at 120 kPa, 26,500 Hz. The *horizontal thin solid line in the lower graph* is the number of Argon molecules in the bubble

evaporates, which leads to a shift between the two collapse times. The lower graph represents the number of water molecules in the bubble, and the horizontal line is the number of argon molecules. In hot water, it is seen that the number of water molecules at the end of the expansion is ten times higher than the number of gas molecules. It is seen that in both cases, some water remains trapped in the bubble after the first collapse, because water transport from the bubble center toward the surface is limited by diffusion through argon. Similar curves can be found in Storey and Szeri (2000). Finally, the collapse temperature for cold water is 9,600 K and drops down to 9,020 K for hot water. This difference would increase with higher drivings.

3.3.6 Relevance to Sonochemistry

Evaporation is fundamental in acoustic cavitation and constitutes the cornerstone of sonochemistry: the solvent contains the "fuel" for the reactions, which, once evaporated in the bubble, is heated by the nearly adiabatic compression, and can be dissociated into radicals, so that the bubble is filled with a mixture of polyatomic species. This process is termed "sonolysis." The endothermic reactions occurring in the bubble also consume a part of the collapse energy and therefore also influence the collapse temperature. Didenko et al. (2000) showed experimentally that by fixing the vapor pressures of octanol and dodecane to the same value, a noticeably hotter collapse was obtained in octanol, which suggests that the octanol expends less energy in its chemical reactions than dodecane.

A simple model in the form of a differential equations system is now available for bubble inertial oscillation accounting for heat and mass transport, and chemistry involving H, C, O, and N (Storey and Szeri, 2001, 2002; Yasui, 2001). This model yields interesting results and confirms some tendencies observed in sonochemistry (see, for example, Storey et al., 2001, for methane formation from water–methanol mixtures).

3.3.7 Measuring Cavitation Temperatures

Suslick and co-workers, in their early works, used reactions of known temperature-dependent kinetics to determine the temperature attained in cavitation bubbles (see Suslick et al., 1999, for a review). A more efficient and reliable method consists in recording the sonoluminescence spectra of species whose emission properties are known, used as thermal probes. The authors used molecular emission of diatomics (C_2) (Flint and Suslick, 1991), or emission from metal atoms (Fe, Cr, Mo) originating from volatile organometallics (McNamara et al., 1999). The comparison of recorded and calculated spectra yields an estimation of the collapse temperature with good accuracy. The order of magnitude of the temperatures attained reaches 5,000 K in some cases.

The temperature attained in SBSL experiments is more difficult to assess since the luminescence spectrum is continuous (although lines could be obtained in some cases) and the emission mechanism is controversial. On the basis of radiative collision processes in a weakly ionized gas, temperatures near 20,000 K have been proposed (Brenner et al., 2002; Hammer and Frommhold, 2000). Recent SBSL experiments in sulfuric acid yielded a 2,700-fold increase in light intensity, and following the authors, the bubble would contain a hot plasma core at 30,000 K (Flannigan and Suslick, 2005; Hopkins et al., 2005).

3.4 Rectified Diffusion

3.4.1 The Physics

As seen in Section 2.5, a quiet bubble in a saturated liquid dissolves, owing to surface tension. When the bubble undergoes radial oscillations, the situation may change. In the expansion phase, the gas pressure in the bubble decreases and so does the dissolved gas concentration at the bubble wall $C_R = p_g(t)/k_g$, by virtue of Henry's law. When the bubble shrinks, the concentration C_R increases. Hence, an oscillating concentration gradient appears in the liquid, resulting in an oscillating diffusion flux. During expansion gas enters in the bubble, and during contraction the bubble loses gas. The process has a non-zero average for the following reasons:

- during expansion, the area for gas exchange is higher, so that there is more gas entering the bubble than gas leaving it during contraction

- because of spherical symmetry and liquid mass conservation, the volume of liquid surrounding the bubble becomes thinner during expansion than during contraction; the outward concentration gradient is thus higher during expansion, and Fick's law predicts a larger inward flux during expansion

Both phenomena predict a net gas accumulation in the bubble over one oscillation cycle and can produce a noticeable bubble growth over many periods. This phenomenon is known as rectified diffusion (RD).

3.4.2 Rectified Diffusion Threshold

The above arguments would predict that an oscillating bubble always grows. In fact, surface tension still promotes dissolution, and a competition takes place between both phenomena. One therefore expects that above a certain oscillation level, the bubble grows, whereby it dissolves in the opposite case. Since the bubble oscillations increase with the driving, this analysis predicts a threshold for bubble growth, termed "rectified diffusion threshold," which defines a curve in the (R_0, p_a) plane. Above the threshold the bubble grows (R_0 increases), while below the threshold it dissolves (R_0 decreases). On the threshold, there is diffusive equilibrium on average, and the bubble keeps a constant R_0. A negative slope of the RD threshold in the (R_0, p_a) plane corresponds to an unstable equilibrium, while positive slope points are stable ones.

3.4.3 Bibliography

The first theoretical treatment dates back to Blake (1949), who did not account for liquid convection. Hsieh and Plesset (1961) proposed the first complete formulation of the problem, and derived an approximate solution for linear oscillations, in good agreement with the measurements of Strasberg (1961). A theoretical breakthrough was performed by Eller and Flynn (1965), who obtained a solution of the problem usable for any bubble dynamics $R(t)$ calculated separately, and opening the theory to non-linear and/or large amplitude oscillations. The mean outward flux across the bubble wall over one period was found to be proportional to the time-averaged concentration difference:

$$\langle C_R \rangle_4 - C_\infty = C_0 \left[\frac{\langle p_g \rangle_4}{p_0} - \frac{C_\infty}{C_0} \right] \tag{2.19}$$

where the notation $\langle . \rangle_4$ refers to the non-linear time average

$$\langle g \rangle_4 = \frac{\int_0^T g(t) R^4(t)\, \mathrm{d}t}{\int_0^T g(t)\, \mathrm{d}t}$$

This expression can be compared with the static case, Equation (2.7). The threshold is obtained for $\langle p_g \rangle_4 / p_0 = C_\infty / C_0$. The average gas pressure $\langle p_g \rangle_4$ decreases as

the bubble oscillation amplitude increases. One therefore expects that the threshold will be lower for any combination of parameters increasing the oscillation amplitude, for example, by increasing the driving, approaching a linear or non-linear resonance, or for inertial oscillations.

Further measurements were carried out by Eller (1972), showing good agreement with the theory of Eller and Flynn (1965) for the threshold. However, the measured growth rates were found to be much higher than predicted by the theory. This was confirmed by Gould (1974), who established a correlation between this abnormally high growth rate with the appearance of bubble shape instabilities. Crum (1980) repeated threshold and growth rate measurements, and also derived analytical expressions of both quantities for linear oscillations, taking into account the damping of the oscillations because of thermal effects in the bubble (see Section 3.3). He found excellent agreement for the threshold, and also for the growth rate for pure water, but noticed that the addition of a small amount of surfactant yielded a fivefold increase of the growth rate without any discernible bubble surface instability. This effect was attributed qualitatively to a layer of surfactant adsorbed at the bubble surface, and was later confirmed theoretically by Fyrillas and Szeri (1995). Crum and Hansen (1982) compared different expressions of the rectified threshold and proposed an interesting discussion on the case of pulsed driving.

The linear threshold of Crum (1980) and Crum and Hansen (1982) is presented in Fig. 2.7. As expected, a strong decrease is visible near the linear resonance. It is important to note that this threshold yields wrong results near non-linear resonances, and also for high drivings, typically near $p_a \simeq p_0$ (see Section 3.4.4).

Church (1988) calculated the rectified diffusion threshold in a wide parameter range, without relying on the hypothesis of linear oscillations. His results showed the existence of various positive slope branches, raising for the first time the possibility of small diffusively stable bubbles. Later, starting a series of papers on the possible effect of surfactants on rectified diffusion, Fyrillas and Szeri (1994) solved in an elegant manner the convection–diffusion problem by perturbation methods,

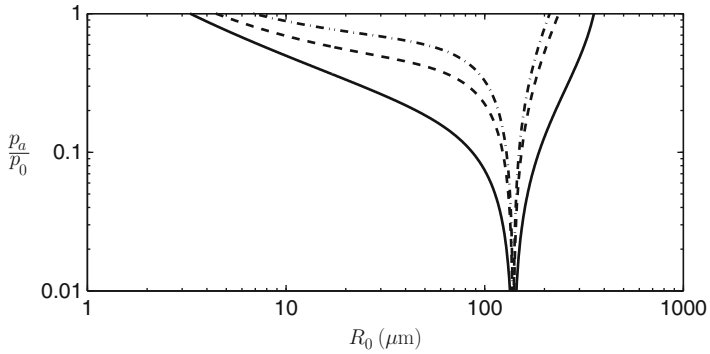

Fig. 2.7 Rectified diffusion threshold based on a hypothesis of linear oscillations. *Solid curve*: $C_1/C_0 = 1$ (saturation); *Dashed curve*: $C_1/C_0 = 0.9$; *Dash-dotted curve*: $C_1/C_0 = 0.8$

and were the first to obtain a consistent expression of the growth rate, valid either near the threshold or not. In a second paper (Fyrillas and Szeri, 1995), they examined the effect of surfactants, possibly resisting gas transport across the bubble interface, and found growth rates in agreement with earlier experiments, strengthening the early hypothesis of Crum (1980). They finally proposed a theoretical formulation for the oscillatory adsorption/desorption process of a surfactant at the surface of an oscillating bubble, and demonstrated that the average quantity of surfactant adsorbed over one period was higher than in the equilibrium case (Fyrillas and Szeri, 1996).

Meanwhile, the first experiments on SBSL revealed the actual existence of a diffusively stable cavitation bubble, neither growing, nor dissolving (Gaitan et al., 1992). This unusual feature in cavitation was investigated by several authors (Akhatov et al., 1997a; Hilgenfeldt et al., 1996; Löfstedt et al. 1995), who calculated that diffusively stable bubbles can be obtained in degassed conditions and that they correspond to the appearance of a positive slope of the rectified diffusion threshold. However, Barber et al. (1995) found that the ranges of dissolved gas concentrations for diffusive stability were lower by a factor 100 in pure argon than in air. The agreement with theory was found good for argon bubbles, but not for air bubbles, for which theory predicted growth instead of the stability observed experimentally. Löfstedt et al. (1995) and Barber et al. (1997) therefore postulated an "anomalous mass flow" necessary to reject more air in the compression phase than predicted by rectified diffusion theory. This key point of SBSL was solved by Lohse et al. (1997) and Lohse and Hilgenfeldt (1997), who proposed that the air in the bubble was heated enough to allow dissociation of O_2 and N_2, the product being easily expelled from the bubble. The air bubble in SBSL experiments were thus found to be in fact an argon bubble (present as 1% in air). This hypothesis is now accepted and has received experimental confirmation (Ketterling and Apfel, 1998; Matula and Crum, 1998). It is interesting to note that the theory of rectified diffusion, almost a half-century after its first theoretical treatment, indirectly supplied a clue to explain this singular chemical effect.

3.4.4 Merging of the Blake and Rectified Diffusion Thresholds for Small Bubbles

Very small bubbles are prevented from oscillating strongly by surface tension, and hence they need a strong driving to become inertial, which is evidenced by the increase of the Blake threshold toward small radii (see left part of Fig. 2.1). If their radial oscillation is so constrained, one may suspect that neither can they grow by rectified diffusion. This therefore suggests that the Blake and rectified diffusion thresholds would almost be the same for small ambient radii.

This is indeed the case, as demonstrated analytically and numerically by Louisnard and Gomez (2003) (this property was already apparent in the results of Church (1988), but remained unnoticed by the latter author). Figure 2.8 shows the RD threshold, computed from the Keller equation (2.10) (thick solid line) for saturated water ($C_\infty = 1$) in a 26.5 kHz acoustic field. Also shown is the threshold

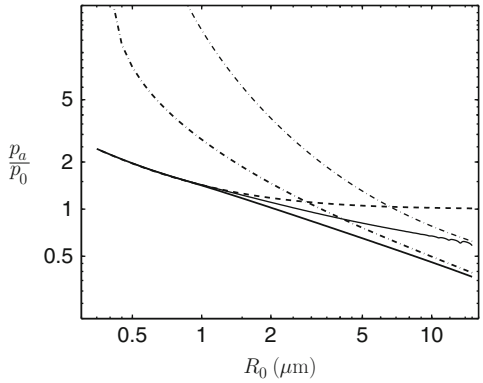

Fig. 2.8 Exact RD threshold for saturated water ($C_1 = 1$) calculated numerically from the Keller equation (*thick solid line*); Blake threshold from Equation (2.5) (*thick dashed line*); and linear theory RD threshold calculated from Crum and Hansen (1982) (*thick dot-dashed line*). The *thin lines* represent respectively the exact (*solid*) and linear (*dot-dashed*) RD thresholds calculated for slightly degassed water ($C_1 = 0.8$). Adapted from Louisnard and Gomez (2003)

calculated from the linear theory (Crum, 1980; Crum and Hansen, 1982, thick dot-dashed line); it is readily seen that for bubbles of small ambient radii, the linear theory fails to predict the pressure threshold value, but for larger bubbles the exact threshold merges with the linear one, at least in the range of radii considered here. The Blake threshold is also represented (thick dashed line), and it is seen that the two curves merge for acoustic pressure greater than, say 1.4 bar, for saturated water. Performing the same calculations for slightly degassed water ($C_\infty = 0.8$) yields the same conclusion, as attested by Fig. 2.8 (the numerical RD threshold is represented by a thin solid line and the linear one by thin dot-dashed line). The computation was also repeated for 50 and 100 kHz frequencies, leading to the same conclusion (not shown).

This feature casts some doubts on what is referred to as the "gaseous cavitation cycle" by Neppiras (1980), which states that small bubbles would grow by rectified diffusion by oscillating in a stable manner ("stable" should be understood in this context as non-inertial) up to the Blake threshold, where they oscillate inertially, break up, and seed new small bubbles. Indeed, for high drivings, the above result indicates that the region in the parameter space for growing non-inertial bubbles is negligible. This might suggest that other growth mechanisms, for example coalescence under secondary Bjerknes forces (Section 5.3.2), may initially participate in the development of the bubble fields (Louisnard, O. (2001). *Theoretical Study of Competition Between Dissolution and Coalescence of Small Bubbles in an Acoustic Field*, "Unpublished"; Louisnard and Gomez, 2003; Mettin, 2005).

Rectified diffusion however occurs in cavitation fields at moderate drivings (say below 100 kPa). In this case, bubbles can indeed grow by rectified diffusion toward large sizes, as attested by the experiments of Crum (1980), and this phenomenon can

be used for degassing applications (Kapustina, 1973). Even for strong drivings, there always exist lower pressure zones in the liquid, where some bubbles can undergo rectified diffusion.

4 Non-spherical Oscillations

4.1 Introduction

Two phenomena prevent the bubble from losing its sphericity: the first one is surface tension and the second is of dynamical origin (we refer the reader to an interesting discussion by Prosperetti, 1999). Conversely, various effects may induce loss of sphericity. First, the environment of the bubble may itself deviate from isotropy. One may think about the influence of a neighboring bubble or a solid boundary, the anisotropy of the acoustic field itself, the effect of gravity that introduces a translational motion, even in the case of levitation experiments, or steady liquid motion. Furthermore, a radially oscillating bubble can develop surface oscillation by an intrinsic shape instability mechanism.

4.2 Shape Instabilities

The dynamic stability of a purely radial motion has been investigated in the early work of Plesset (1949). The local bubble radius is expanded as the sum of spherical harmonics:

$$r(\theta,\phi,t) = R(t) + \sum_{n=1}^{\infty} a_n(t) Y_n(\theta,\phi) \tag{2.20}$$

Assuming potential flow, writing the continuity equations at the bubble interface and performing a linear stability analysis yields

$$\ddot{a}_n + \frac{3\dot{R}}{R}\dot{a}_n - (n-1)\left[\frac{\ddot{R}}{R} - (n+1)(n+2)\frac{\sigma}{\rho_l R^3}\right] a_n = 0 \tag{2.21}$$

The mode $n = 1$ corresponds to a translational motion of the spherical bubble with a velocity $v = \dot{a}_1$. For n>2, the second term in the square bracket shows that surface tension has a stabilizing role, increasing with the mode number. The first term has a destabilizing role when $\ddot{R} > 0$, that is, when the acceleration is oriented from the gas toward the liquid. This is the classical statement of the Rayleigh–Taylor instability, originally derived for a plane interface. Here, it can appear at the end of the collapse, as the bubble rebounds, where $\ddot{R}$ can reach huge values. Its occurrence is thought to limit the stability region of SBSL for increasing drivings p_a (see below). The second term in Equation (2.21) is seen to act as a negative damping

when $\dot{R} < 0$, that is, when the bubble is collapsing (Plesset and Mitchell, 1956), and therefore favors instability during the bubble collapse.

Another type of instability, termed "parametric" or "Faraday instability" (well known in the case of a plane interface), accumulates over time because of the periodic character of the square bracket in Equation (2.21). Figure 2.9 exhibits short exposure photographs of cavitation bubbles undergoing this type of instability (Kornfeld and Suvorov, 1944).

Fig. 2.9 Snapshots of shape instable bubbles. Reused with permission from Kornfeld and Suvorov (1944, p. 495). Copyright 1944, American Institute of Physics

Parametric instabilities have been correlated with an erratic translational motion of the bubble by Eller and Crum (1970) for drivings lower than 70 kPa, near 20 kHz. Their approximate calculations of thresholds for parametric instability compares reasonably with the measured thresholds for erratic drift.

The theory of Plesset has been extended by Prosperetti (1977b) to account for viscous effects, and simplified in the limit where viscous effects are concentrated in a diffusion layer near the bubble (Hilgenfeldt et al., 1996; Prosperetti and Seminara, 1978).

4.3 Stability Thresholds

In SBSL experiments, when p_a is increased, the sonoluminescing bubble suddenly disappears (near $p_a = 150$ kPa, Gaitan et al., 1992). This is attributed to the appearance of Rayleigh–Taylor instability as the bubble collapses. Besides, in the same experiments, if water is not degassed enough, bubbles may grow by rectified diffusion (emitting SL) up to a critical size (near 5 μm) where they break, pinch-off a microbubble, and start to grow again (this process is known as unstable SBSL). The upper critical size is found theoretically to correspond to parametric instabilities.

To explain these findings, Brenner et al. (1995), Hilgenfeldt et al. (1996), and Brenner et al. (2002) established the region in the parameter space where stable and unstable SBSL can be obtained. From this formulation, they sought the domain in the parameter space (R_0, p_a), where the bubble remains spherical against both parametric and Rayleigh–Taylor instability. The former was found to limit the stability domain toward increasing R_0, while the latter did so for increasing p_a.

The obtained results were then refined by several authors, taking into account the variations of the gas density during collapse (Lin et al., 2002b; Yuan et al., 2001), and/or using a more realistic model for the bubble radial oscillations. The latter

point is crucial especially for predicting the Rayleigh–Taylor instability threshold, which is very sensitive to the precise value of $\ddot{R}$ at the end of the collapse. Prosperetti and Hao (1999) showed that accounting for thermal effects in the gas reduced $\ddot{R}$ sufficiently to suppress the Rayleigh–Taylor instability in the SBSL range of parameters. The same conclusion was reached by Augsdorfer et al. (2000) and Yuan et al. (2001), while Lin et al. (2002b) recalculated the instability thresholds accounting for variations of gas density and for thermal effects and water transport at the bubble wall (Storey and Szeri, 2001). For the Rayleigh–Taylor threshold, they found a convincing agreement with the experiments of Ketterling and Apfel (2000).

Although initially relevant to SBSL, these thresholds are also of great importance for cavitation fields. Anisotropy is more important in multibubble fields than in single-bubble levitation experiments, so that, for the same drivings, the values of R_0 calculated or measured in the latter context may be considered as upper boundaries for bubble sizes in cavitation fields. In connection with this issue, we would like to mention the experimental work of Gaitan and Holt (1999), who measured the parametric instability threshold in a 20 kHz levitation cell for a wide range of driving p_a (Fig. 2.10). The points clearly define an upper bound for the ambient radius for a given driving. The resonant radius at 20 kHz is 150 μm, and it is clear from these measurements that no resonant bubble can survive even for relatively low drivings. Even for p_a as low as 30 kPa, it is seen that bubbles would undergo shape instability near 60 μm.

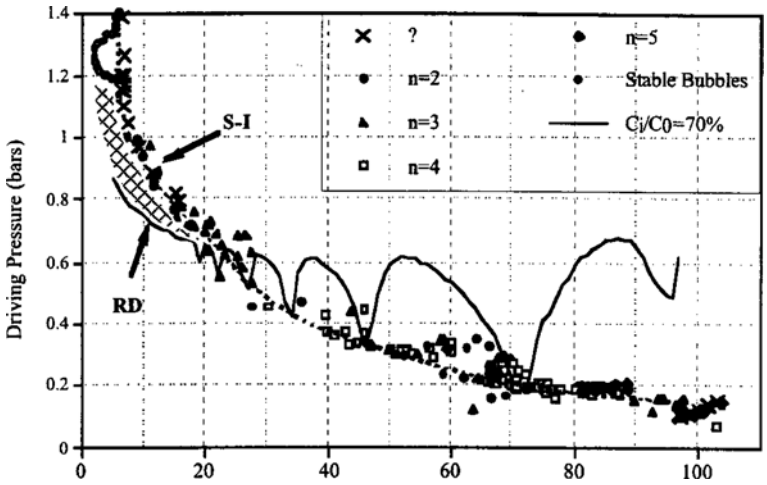

Fig. 2.10 Instability threshold measured in a 20 kHz levitation cell. The *different symbols* indicate the order of the unstable mode recorded by image processing. The *cross symbols* correspond to an instability whose order could not be determined. The *solid line* is the calculated rectified diffusion threshold for $C_1/C_0 = 0.7$. Reprinted Fig. 2.2 with permission from Gaitan and Holt (1999). Copyright (1999) by the American Physical Society

4.4 Self-Propulsion of Non-spherical Bubbles

Common observation of cavitation fields reveals bubbles undergoing erratic dancing motions. It was first suggested by Strasberg and Benjamin (1958) that this translation motion could originate from surface instabilities. As mentioned above, this has been confirmed experimentally by Eller and Crum (1970), who observed that the measured driving threshold for this behavior to occur coincided with the calculated threshold for parametric surface instabilities. The problem has been tackled theoretically by Benjamin and Ellis (1990) and Zardi and Seminara (1995), who showed that the translation motion could appear by a non-linear coupling between two adjacent instability modes. More recent treatment (Doinikov, 2004; Reddy and Szeri, 2002) generalized this result.

4.5 Non-spherical Collapses Near Boundaries and Erosion

A bubble collapsing near another bubble or near a solid surface undergoes a non-spherical collapse. The astonishing variety of shapes attained by these bubbles constitutes a scientific challenge, both theoretically and experimentally, owing to the short deformation timescales involved in the collapse. The main motivation for investigating non-spherical collapses dates back to the original issue of solids damaging by hydrodynamic cavitation bubbles. As noted by Lauterborn et al. (1999), no material has been found to resist their attack, a rather peculiar effect, if one intuitively thinks of bubbles as soft objects. The issue is of importance not only for erosion of propellers, blades, and hydraulic systems, but also for acoustic cavitation whose erosion effect is well known and generally damages the tip of the transducer.

The analysis of Rayleigh outlined that the high pressures, possibly as shockwaves, generated by a spherical implosion were the origin of erosion. Since then, it appeared that the impact of high-speed liquid jets, formed by the involution of collapsing cavities, could be a primary factor in cavitation damage. The important pioneering experimental and theoretical study of Benjamin and Ellis (1966) stated the problem in terms of the important concept of Kelvin impulse and presented images of spark-induced bubbles. Other results on spark-induced bubbles near boundaries can be found in the literature, but better reproducibility and precision in the location of the bubble can be obtained with laser-generated bubbles since the early experiments of Lauterborn and Bolle (1975).

The phenomenon can be seen in the photographic series in Fig. 2.11 from Lauterborn et al. (1999). The bubble involutes from the top, and the downward liquid jet develops, pushes the lower boundary of the bubble toward the solid surface, impinging on it violently, which creates a pit just below the bubble. On some occasions, the jet can pierce the bubble, which becomes a torus, and further disintegrates into a circle of small bubbles, whose implosion generates a circle of pits. The behavior is reproducible for a fixed ratio between the boundary-bubble separation and the maximum bubble radius. More experimental facts, including complex shockwaves

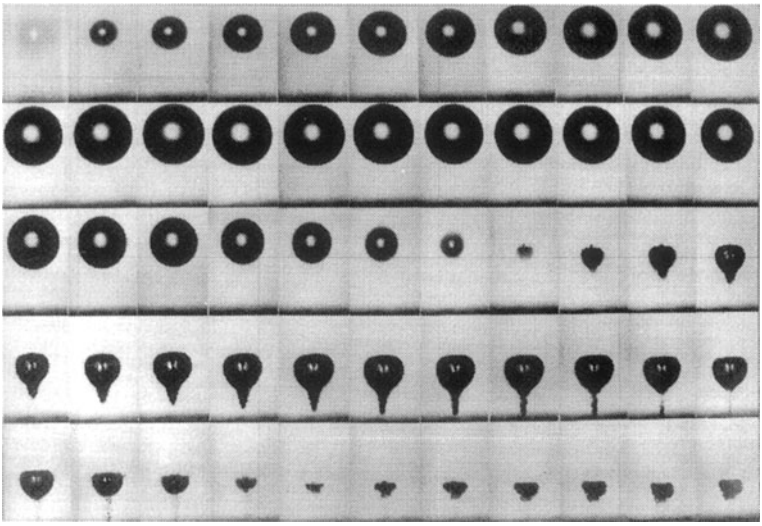

Fig. 2.11 Non-spherical collapse of a laser-induced bubble near a flat rigid boundary, recorded at 75,000 frames per second. The solid boundary is below the bubble. Adapted from Lauterborn et al. (1999), with kind permission of John Wiley and Sons Ltd

formation, can be found in Philipp and Lauterborn (1998), Lauterborn et al. (1999), and Lindau and Lauterborn (2003).

Erosion by acoustic cavitation is also well known, but is infinitely more difficult to control than laser bubbles. Recent experiments show that within the same experiment, the various bubble structures that emerge from the acoustic field (see Section 5.4) have different erosion effects (Krefting et al., 2004). Unlike laser experiments that allow the precise positioning of the bubble, acoustic cavitation bubbles can rise up from various places, and the solid boundaries themselves can act as bubble sources. Laser bubble experiments therefore constitute a perfect tool to assess the complex phenomena involved, and the precise mechanisms of damaging at the scale of a single bubble.

4.6 Non-spherical Collapses Far from Boundaries

Non-spherical collapses can also occur without the presence of a solid boundary. First by symmetry, a bubble collapsing at a distance s of a solid boundary problem is equivalent to the problem of two identical bubbles collapsing at a distance $2s$. This is confirmed by experiments of Lauterborn et al. (1999).

But a single bubble can also collapse non-spherically and form liquid jets because of its translational motion. This is supported by the experiments of spark-induced bubble with or without gravity (Benjamin and Ellis, 1966) and theoretically (Blake and Gibson, 1987; see also Prosperetti, 1999), on the basis of impulse conservation.

Even in levitation experiments, this is also the case because the bubble undergoes a small, but non-zero, translational motion, owing to gravity. It has been suggested that sonoluminescing bubbles could in fact collapse non-spherically, and that the corresponding liquid jet could be responsible for the light emission (Prosperetti, 1997). It was found, however, that under microgravity, where jets would be unexpected, even more light was emitted (Matula, 2000), and also that light emission decreases and even ceases with increasing asphericity (Ohl et al., 1998).

Whether or not aspherical collapses indeed occur in single bubble experiments remains an open question. In multibubble fields, it is generally accepted that the bubbles collapse aspherically, but this is difficult to assess experimentally. Another issue relevant to this discussion is the difference of light emission spectra between single- and multi-bubble sonoluminescence. Without entering into this complex problem, we would like to mention the experiments of Matula et al. (1995). The sonoluminescence spectrum of NaCl–water mixtures reveals that the sodium line emission is present in multi-bubble sonoluminescence (MBSL), and absent in SBSL. Since sodium cannot evaporate into the bubbles, this may suggest that droplets of solution could enter the bubble during a surface instability process or aspherical collapse with jetting. Therefore, one of the latter processes would necessarily occur in multi-bubble conditions. This is an important point, since it means that non-volatile species could also participate in this way to chemical reactions in the hot gaseous environment inside the bubble.

5 Cavitation Fields

5.1 Acoustics

5.1.1 Equation of Linear Acoustics

Linear acoustics refers to non-dissipative low amplitude sound propagation. Thus it may not be the relevant tool to study cavitation, since the latter converts acoustic energy into various forms of energy (thermal, interfacial or light). However, some basic concepts can be used profitably, on one hand to design sonoreactors, and on the other hand to characterize cavitation experiments.

The linear propagation of an acoustic wave results from the isotropic elastic properties of the liquid. When the liquid is expanded or compressed, an elastic force tends to restore equilibrium, and in doing so, accelerates the liquid. Non-dissipative acoustic waves can be described by linearized Euler equations, neglecting viscosity:

$$\frac{\partial p}{\partial t} + \rho_l c_l^2 \nabla . \mathbf{u} = 0 \tag{2.22}$$

$$\rho_l \frac{\partial \mathbf{u}}{\partial t} = -\nabla p \tag{2.23}$$

where $\mathbf{u}(\mathbf{x}, t)$ is the liquid velocity field associated to the acoustic wave, and $p(\mathbf{x}, t)$ the local acoustic pressure. This set of equations can be reduced to a propagation equation

$$\nabla^2 p - \frac{1}{c_l^2}\frac{\partial^2 p}{\partial t^2} = 0 \tag{2.24}$$

Various boundary conditions may be associated to this equation. Among the simplest, either the pressure or the velocity can be prescribed. An infinitely soft boundary is represented by p=0, and an infinitely rigid one by $\mathbf{u}.\mathbf{n} = \mathbf{0}$, where $\mathbf{n}$ is the outward unit vector normal to the boundary.

Assuming mono-harmonic waves at frequency ω, and using complex notation

$$p = \frac{1}{2}\left[p_\mathrm{a}(\mathbf{x})\mathrm{e}^{\mathrm{i}\omega t} + \mathrm{c.c.}\right], \qquad \mathbf{u} = \frac{1}{2}\left[\mathbf{u_a}(\mathbf{x})\mathrm{e}^{\mathrm{i}\omega t} + \mathrm{c.c.}\right] \tag{2.25}$$

where c.c. denotes the complex conjugate. Equation (2.24) reduces to the Helmholtz equation

$$\nabla^2 p_\mathrm{a} + k_\mathrm{l}^2 p_\mathrm{a} = 0 \tag{2.26}$$

where $k_\mathrm{l} = \omega/c_\mathrm{l}$ is the wavenumber.

5.1.2 Energy Conservation: Non-dissipative Acoustics

An energy conservation equation can be deduced from Eqs. (2.22) and (2.23):

$$\frac{\mathrm{d}}{\mathrm{d}t}\int\int_V\int\left(\frac{1}{2}\rho_\mathrm{l}u^2 + \frac{1}{2}\frac{p^2}{\rho_\mathrm{l}c_\mathrm{l}^2}\right)\mathrm{d}V = \int\int_S -p\mathbf{u}\mathbf{n}\,\mathrm{d}S \tag{2.27}$$

where V is an arbitrary volume of fluid and S its boundary. The parenthesis in the volume integral is the acoustic energy density (in W m^{-3}), which is the sum of the kinetic and potential compressional energy of the liquid, and $p\mathbf{u}$ is called acoustic intensity (in W m^{-2}). Both are local quantities. Equation (2.27) expresses that the variations of acoustic energy in a volume result from the difference between the fluxes of mechanical energy entering and leaving this volume, and result directly from the theorem of kinetic energy.

For mono-harmonic waves, it can be easily checked that the left side of Equation (2.27) is zero on average over one acoustic period. Besides, the average acoustic intensity $p\mathbf{u}$ can be shown to read $\Re(p_\mathrm{a}\mathbf{u_a})/2$, where $\Re$ denotes the real part of a complex number. Now, let us consider the case of a sonoreactor excited by the vibrating surface $S_\mathrm{sonotrode}$ of a sonotrode, and closed by boundaries $S_\mathrm{boundaries}$, of unspecified type for now. Equation (2.27) becomes

$$\underbrace{\int\int_{S_{\text{sonotrode}}} -\frac{1}{2}\Re(p_{\text{a}}\mathbf{u_a}).\mathbf{n}\,\mathrm{d}S}_{\substack{P_{\text{active}}=\text{ power}\\(>0)\text{ emitted}\\\text{into the liquid}}} = \underbrace{\int\int_{S_{\text{boundaries}}} \frac{1}{2}\Re(p_{\text{a}}\mathbf{u_a}).\mathbf{n}\,\mathrm{d}S}_{\substack{P_{\text{bound}}=\text{ power}\\(>0)\text{ lost}\\\text{through the}\\\text{boundaries}}} \tag{2.28}$$

The left integral is the power transmitted from the sonotrode to the liquid, and is termed *active power*. The above relation states that all the mechanical energy entering the liquid is lost by boundaries. In the case of perfect rigid or soft boundaries, Equation (2.28) merely states that the acoustic power transmitted to the liquid by the sonotrode is zero. This a priori paradoxical result originates from the non-dissipative character of the medium, which is implicitly assumed in Eqs. (2.23) and (2.24).

5.1.3 Energy Conservation and Dissipation: Calorimetric Method

Various physical processes can yield attenuation of acoustic waves, including viscosity or finite thermal diffusion, among others. In the case of bubbly liquids, the main dissipation occurs at the bubble level (see Sections 3.2.3 and 5.1.4). Whatever its physical origin, attenuation of mono-harmonic linear waves (or their superposition) can be modeled by introducing a complex wavenumber

$$k = k_{\text{l}} - \mathrm{i}\alpha \tag{2.29}$$

in (2.26), where $\alpha > 0$ is the attenuation coefficient in m^{-1}. In this case, it can be shown that Equation (2.28) becomes

$$\underbrace{\int\int_{S_{\text{sonotrode}}} -\frac{1}{2}\Re(p_{\text{a}}\mathbf{u_a}).\mathbf{n}\,\mathrm{d}S}_{\substack{P_{\text{active}}=\text{ power}\\(>0)\text{ emitted}\\\text{into the liquid}}} = \underbrace{\int\int_{S_{\text{boundaries}}} \frac{1}{2}\Re(p_{\text{a}}\mathbf{u_a}).\mathbf{n}\,\mathrm{d}S}_{\substack{P_{\text{bound}}=\text{ power}\\(>0)\text{ lost}\\\text{through the}\\\text{boundaries}}} + \underbrace{\int\int\int_{V} \alpha\frac{|p_{\text{a}}|^2}{\rho_{\text{l}}c_{\text{l}}}\,\mathrm{d}V}_{\substack{P_{\text{diss}}=\text{ power}\\(>0)\text{ dissipated}\\\text{in the liquid}}} \tag{2.30}$$

For perfectly reflecting boundaries, this equation now states that the period-averaged power sent through the sonotrode surface is the power dissipated in the liquid.

The integral P_{diss} represents the opposite of the power of internal dissipative forces (for example viscous friction). Combining the theorem of kinetic energy with the first principle of thermodynamics, it can be shown that

$$\int\int\int_V \rho_\mathrm{l} C_{v_\mathrm{l}} \frac{\mathrm{d}\langle T\rangle}{\mathrm{d}t} = P_\mathrm{diss} + \dot{Q} \tag{2.31}$$

where V is an arbitrary volume of insonified liquid, $\langle T\rangle$ is the local temperature of the liquid averaged over one or more acoustic periods, and $\dot{Q}$ is the (algebraic) heat gained or lost by volume V. This equation is the basis of the so-called calorimetric method. Taking V as the whole volume of insonified liquid, and stirring sufficiently to ensure uniform temperature, $\langle T\rangle$ is monitored in a given point of the sonoreactor by a temperature probe as soon as ultrasound is switched on. At $t = 0$ heat cannot escape owing to thermal inertia, so that $\rho_\mathrm{l} C_{v_\mathrm{l}} \langle \mathrm{d}T/\mathrm{d}t\rangle_{t=0}$ matches P_diss. Thus, the initial slope of the temperature curves yields an estimation of the power dissipated in the liquid, which, from Equation (2.30), is also the active power sent through the sonotrode area. This calorimetric method is easy to use and is commonly used to characterize cavitation experiments (Ratoarinoro et al., 1995). Finally, it should be noted that the quantity $|p_a|^2/(\rho_l c_l)$ is sometimes improperly termed "intensity." We emphasize that this is true only for plane traveling-wave, but is definitely not in other cases.

5.1.4 Acoustics of Bubbly Liquids

The presence of bubbles in a liquid increases the compressibility of the effective medium. Therefore, one expects the effective sound velocity to decrease. This is indeed the case for low-frequency waves or small bubbles. As the frequency or the bubble radius increases, the phase shift between the bubble response and the local driving pressure leads to a variation of the effective sound speed. The latter therefore varies with frequency, and waves in such a medium are called dispersive. Moreover, the non-linear behavior of the bubbles oscillation renders high-intensity waves non-linear.

Theory of bubbly liquids acoustics can be traced back to Foldy (1944) and Carstensen and Foldy (1947). Their result contains the main physics and is equivalent to the most recent theories in the linear case, and at low gas fractions. Linear experimental data were recorded by Fox et al. (1955) and Silberman (1957), the latter report still constituting a reference. Theory for non-linear waves has been derived independently by van Wijngaarden (1968) and Iordansky (1960), and a similar model, based on a rigorous averaging method, was derived by Caflish et al. (1985). Commander and Prosperetti (1989) developed a linear form of this model, extending it to polydisperse bubble populations and compared it to the experiments of Silberman.

The Caflish propagation equation reads

$$\frac{1}{c_\mathrm{l}^2}\frac{\partial p}{\partial t} - \nabla^2 p = \rho_\mathrm{l}\frac{\partial^2}{\partial t^2}\int_0^\infty N(\mathbf{x}, R_0)\frac{4\pi}{3}R^3[p(t), R_0]\,\mathrm{d}R_0 \tag{2.32}$$

where $N(\mathbf{x}, R_0)\mathrm{d}R_0$ is the number of bubbles per unit volume, in the range of sizes $[R_0, R_0 + \mathrm{d}R_0]$, located at $\mathbf{x}$, and $R[p(t), R_0]$ is the radial dynamics of a bubble of ambient radius R_0 excited with the local acoustic pressure $p(t)$, obtained from Equation (2.10) for example. The integral can be recognized as the instantaneous bubble volume fraction.

Equation (2.32) is intrinsically non-linear, but assuming mono-harmonic low-amplitude waves and using the linear theory of bubble oscillations exposed in Section 3.2.3, the Caflish model reduces to an Helmholtz equation $\nabla^2 p_\mathrm{a} + k^2 p_\mathrm{a} = 0$ with $k^2 = (\omega/c)^2$, and

$$\frac{1}{c^2} = \frac{1}{c_1^2} + 4\pi \int_0^{+\infty} \frac{R_0}{\omega_0^2(R_0) - \omega^2 + 2\mathrm{i}b(R_0)\omega} N(\mathbf{x}, R_0)\, \mathrm{d}R_0 \tag{2.33}$$

where ω_0 and b are given by Eqs. (2.13) and (2.14). It should be noted that k and c are now complex quantities, which implies a spatial wave attenuation (see Section 5.1.3). Moreover, both depend on frequency, traducing the dispersive character of the medium. From expression (2.33), the following conclusions can be drawn:

- For $\omega \ll \omega_0$, the sound speed in the bubbly liquid is lower than the sound speed in the pure liquid. This was expected owing to the larger compressibility of the medium.
- As ω approaches ω_0, the sound speed decreases drastically. Just above ω_0, c^2 becomes negative, so that the sound velocity has a large imaginary part, which produces strong attenuation of the waves. Physically, this peculiar result comes from the fact that above resonance, the bubble contracts in the expansion phase of the acoustic pressure (Section 3.2.3). Thus, all happens as if the bubbles had a negative compressibility.
- For increasingly large frequencies, the oscillation of the bubbles vanishes and the sound speed of the pure liquid is recovered.

It should be emphasized that the bubble size distribution N must be known if one wishes to calculate the effective sound speed c. Various studies solved the linear Caflish model in order to predict the sound field in sonoreactors (Dähnke et al., 1999; Servant et al., 2000, 2003), but used an arbitrary Gaussian distribution, involving bubbles much larger than experimentally observed (see Section 5.4.5), so that the validity of the predictions is difficult to assess. In fact, some of these results show negligible departure from linear acoustics, owing to the small bubble fractions introduced in the model.

5.2 Nucleation of Bubbles

As seen in Section 2.5, a spherical gas bubble is unstable in a saturated quiet liquid, and must dissolve. This questions the origin of the numerous cavitation bubbles observed shortly after switching on the sound field.

The theoretical tensile strength of pure water, which is the lowest negative pressure it can support without homogeneous nucleation of a cavity, is −100 MPa. The lowest measured tensile strength reaches −27 MPa (Briggs, 1950). This is still well below the negative acoustic pressures that can be reached with ultrasound. Thus, the bubbles originate necessarily from existing gas pockets, stabilized in the liquid in some way.

The first explanation is that free gas nuclei exist in the liquid, protected against dissolution by a shell of either hydrophobic ions or surface active species. The second explanation postulates that gas nuclei can remain trapped in the crevices of solid impurities or of the vessel wall. Both hypotheses are supported by experimental results. We refer the reader to the reviews of Crum (1982) and Apfel (1984).

It should be added that the size and location of such nuclei is an unknown data, and is one of the main limits to observation of acoustic cavitation. Single-bubble levitation experiments and laser bubbles may remedy this uncontrollable feature.

5.3 Forces Exerted on the Bubbles

5.3.1 Primary Bjerknes Force

Let us seek the force that would be exerted on the bubble if it were replaced by liquid, in otherwise equal conditions. Neglecting viscous effects, it reads

$$\mathbf{F} = \int\int_S -p\mathbf{n}\,\mathrm{d}S \tag{2.34}$$

where S is the bubble surface and p the local pressure on this surface. Using divergence theorem, one may also write

$$\mathbf{F} = \int\int\int_V -\nabla p\,\mathrm{d}V \tag{2.35}$$

where p should be understood as the pressure field that would exist *in the liquid replacing the bubble*. If the fluid is only submitted to the gravity field, $\nabla p = \rho_\mathrm{l}\mathbf{g}$, and we recover the buoyancy force $\mathbf{F_A} = -\rho_\mathrm{l} V\mathbf{g}$. If the pressure field now results from the acoustic wave, but varies little at the scale of the bubble (this implies $R/\lambda \ll 1$), ∇p can be considered as homogeneous in V and equal to its value at the bubble center, hence $\mathbf{F} = -V\nabla p$. This is the instantaneous primary Bjerknes force. For a radially oscillating bubble in an acoustic field, both V and ∇p are oscillating quantities, and the average of their product over one period may be different from zero, so that the bubble experiences an average force. The so-called primary Bjerknes force is this time average,

$$\mathbf{F_{B_1}} = -\langle V(t)\nabla p\rangle \tag{2.36}$$

and may be seen as a generalized buoyancy force in an accelerating liquid. Assuming a mono-harmonic standing wave, the acoustic field can be written as

$$p(\mathbf{x}, t) = p_{\mathrm{a}}(\mathbf{x})\, cos(\omega t) \tag{2.37}$$

so that the primary Bjerknes force becomes

$$\mathbf{F_{B_1}} = -\nabla p_{\mathrm{a}} \langle V(t) cos(\omega t) \rangle \tag{2.38}$$

It is seen that the force points toward pressure nodes (minima) or pressure antinodes (maxima), depending on the sign of the average. In the case of linear oscillations, the Bjerknes force can be easily evaluated from Equations (2.11) and (2.12), and the following conclusions can be drawn:

- for $R_0 < R_{\mathrm{res}}$, bubbles are attracted toward pressure antinodes
- for $R_0 > R_{\mathrm{res}}$, bubbles are attracted toward pressure nodes

Repulsion of bubbles larger than R_{res} has been reported by Goldman and Ringo (1949), and can be observed easily in most cavitation experiments, where large (and therefore visible) bubbles can be seen to escape and take refuge far from pressure antinodes, possibly coalesce, and then rise by buoyancy.

Attraction of bubbles smaller than resonance size by pressure antinodes is confirmed by the experiments of Crum and Eller (1970) for moderate drivings, and is used to levitate a bubble in SBSL experiments, the primary Bjerknes force compensating exactly the mean buoyancy force at a point slightly above the pressure antinode in the center of the cell (Barber et al., 1997; Gaitan et al., 1992).

However, it was shown by Akhatov et al. (1997b) that the primary Bjerknes force can also become repulsive for sub-resonant bubbles, above a threshold in the (p_{a}, R_0) plane. For example, bubbles of 10 μm are repelled by antinodes for drivings exceeding 170 kPa, in contradiction with linear theory. This has been confirmed by experiments (Parlitz et al., 1999) and is illustrated in Fig. 2.12. The inversion of primary Bjerknes force has also been invoked to explain the upper limit of the driving observed in SBSL experiments.

Finally, let us note that Bjerknes forces also exist in traveling waves, and may become important for large drivings. They could explain the conical bubble filaments observed under the transducer tip (Moussatov et al., 2003a), as mentioned recently by Koch et al. (2004b).

5.3.2 Secondary Bjerknes Force

The arguments leading to the expression of the primary Bjerknes force can be extended to the case where the bubble also experiences the acoustic field radiated by a second bubble. The resulting force averaged over one period reads

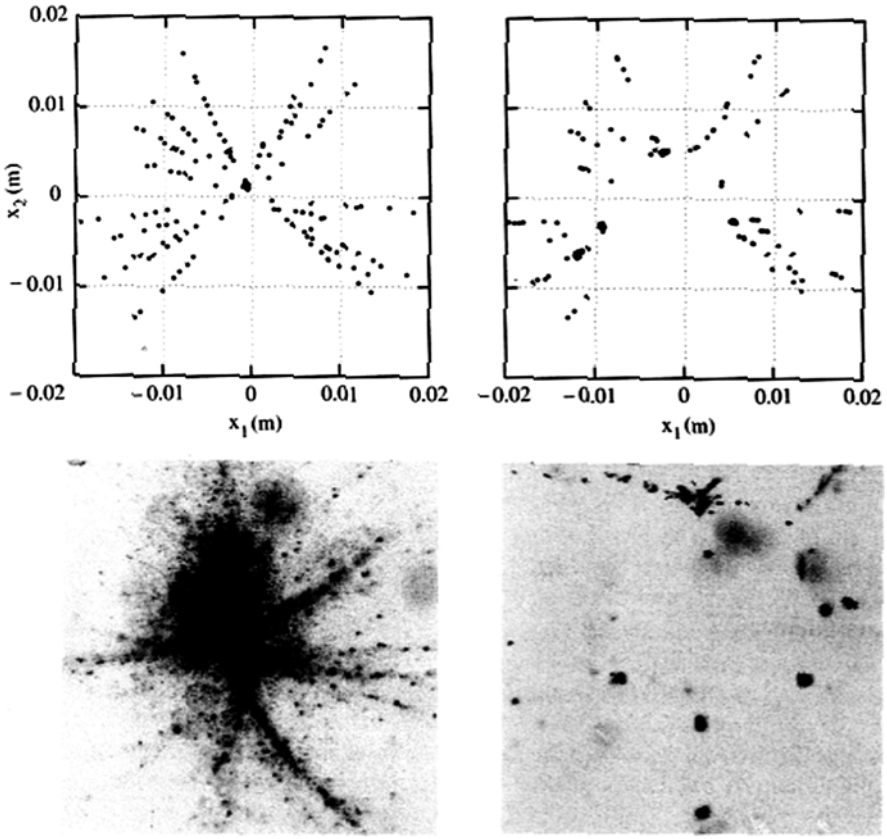

Fig. 2.12 Bubble filaments in a standing wave field. *Upper graphs*: simulations by a particle model. *Lower photos*: snapshots of experimental structures. The *left column* is obtained for a driving of 130 kPa, the *right one* for 190 kPa. The inversion of the Bjerknes force is apparent on the *right graphs*. Adapted from Lauterborn et al. (1999), with kind permission of John Wiley and Sons Ltd

$$\mathbf{F}_{\mathbf{B_2}} = -\frac{\rho_l}{4\pi}\langle \dot{V}_1 \dot{V}_2 \rangle \frac{\mathbf{x}_2 - \mathbf{x}_1}{|\mathbf{x}_2 - \mathbf{x}_1|} \tag{2.39}$$

where V_1, V_2 are the respective volumes of the bubbles, and $\mathbf{x}_1$ and $\mathbf{x}_2$ the spatial positions of their centers. Here again, a practical result is readily obtained in the case of linear oscillations:

- a bubble smaller than and a bubble larger than resonance size repels each other
- two bubbles smaller or two bubbles larger than resonance size experience an attracting force

The experiments of Crum (1975) confirm that the attraction of two sub-resonant bubbles for moderate drivings and quantitative agreement is obtained for the

bubble velocities. The effect of shape instabilities has been tackled by Pelekasis and Tsamopoulos (1993), and the effects of non-linearity have been studied by Oguz and Prosperetti (1990) and Mettin et al. (1997). The latter recalculated the secondary Bjerknes force for non-linear bubble dynamics, and predicted amplitudes orders of magnitude greater than with linear theory for bubbles ranging from 0.5 to 10 μm. An outstanding experimental confirmation of the theory, using laser-induced bubbles in a standing wave, can be found in Koch et al. (2004a)

Mettin et al. (1997) also found that possible mutual repulsion could occur, where linear theory predicts the opposite. Furthermore, the transition from attraction to repulsion can theoretically occur as the bubbles approach mutually, so that a stable separation distance could exist. The result is of importance in the context of bubble structures (see Section 5.4).

5.3.3 Added Mass and Viscous Drag Force

Bubble inertia is negligible, owing to the low density of the gas. However, as any body accelerating relatively to the liquid, a bubble must push the latter, and in reaction experiences a force from it. All happens as if the bubble had an added mass, which for a spherical body always amounts to half the mass of the displaced liquid (Magnaudet, 1997), so that

$$\mathbf{F_M} = -\frac{2}{3}\pi\, R(t)^3 \rho_l \frac{\mathrm{d}}{\mathrm{d}t}(\mathbf{v} - \mathbf{u}) \tag{2.40}$$

where $\mathbf{v}$ is the bubble velocity.

The bubble also experiences a viscous drag force from the liquid. The correct expression of the drag force on a bubble moving radially is a delicate issue. For high-Reynolds numbers, calculated either from the radial or the translational velocity, Magnaudet and Legendre (1998) showed that

$$\mathbf{F_V} = -12\pi\, R(t)\mu_l(\mathbf{v} - \mathbf{u}) \tag{2.41}$$

This completes the set of forces exerted on cavitation bubbles. Since the bubble inertia is negligible, the sum of these period-averaged forces must cancel. This yields a differential equation whose resolution allows a theoretical prediction of the bubble path. Good quantitative agreement with two bubbles experiments has recently been obtained by Koch et al. (2004a).

5.4 Bubble Structures

An immediate conclusion can be drawn from the naked-eye observation of acoustic cavitation: the bubble spatial repartition is neither homogeneous nor stationary. Bubbles self-organize in a variety of different patterns, evolving on a timescale much larger than the acoustic period.

Early observations report mainly two main classes of bubble structures: streamers (Neppiras, 1980; Nyborg and Hughes, 1967) and clusters (Rozenberg, 1971b; Sirotyuk, 1971), but these reports were penalized by a lack of sufficient imaging techniques. Since then, the group of Lauterborn has recorded an impressive collection of experimental data, using high-speed cameras and holographic systems, combined with digital image processing. An extensive review of these observations can be found in Mettin (2005) and references herein, establishing a "zoo" of bubble structures. We summarize in a few words the characteristics of some of these structures and their interpretation in terms of Bjerknes forces.

5.4.1 Streamers and Filaments

The basic streamer is a linear streak of bubbles traveling rapidly from one end to the other. The streamer seems to start from a specific point in the liquid. This structure appears in standing waves configurations at moderate drivings. The origin of the streamer corresponds to a pressure node and the bubbles travel toward pressure antinodes, under the influence of the primary Bjerknes force. Secondary Bjerknes forces act at various levels: they may help nuclei to coalesce near the streamer origin, and maintain an attraction between a bubble and its neighbors in the streamer. Bubbles are thought to break up as they reach the antinode, or form clusters.

Streamers can combine and form slowly evolving agglomerates of filaments, termed "Acoustic Lichtenberg Figures" by Lauterborn's group (Fig. 2.12). The main features of these structures have been explained theoretically by particle model simulations (Parlitz et al., 1999; see also Section 5.5).

5.4.2 Bubble Layers: The Jellyfish and the Starfish

This jellyfish structure consists of two flat parallel layers of bubbles, presenting filamentary structures when viewed from above. They appear in standing waves at high amplitudes, and the layers are located symmetrically on each side of a nodal plane. The layers are not located exactly at the antinodes; this confirms the repulsive character of primary Bjerknes force for high drivings. The estimated driving at the bubble locations is about 200 kPa, and the bubbles involved do not exceed a few micrometers. The starfish structure shares some similarities with the jellyfish, except that it is located near the liquid surface. Both structures are also predictable by particle models.

5.4.3 Clusters

Small clusters of a few (up to some dozens) bubbles appear for large drivings (between 190 and 300 kPa). They can form at the end of a filament. The bubbles constituting the cluster change their positions, can split or merge, and their separation is of the order of their maximum size. The cluster as an entity is a rather stable structure, and reacts to Bjerknes forces as if it were a single large bubble. Why the

bubbles constituting the cluster do not coalesce under secondary Bjerknes force is not completely understood.

Large clusters contain hundreds of bubbles of sizes and mutual distances comparable to small ones. They have a noticeable spherical shape, appear spontaneously in the liquid and travel rapidly. They are attracted by the surface to which they remain attached, taking a hemispherical form, and have a strong eroding action.

5.4.4 Sonotrode Cavitation and Conical Structures

Small diameter sonotrodes, commonly used in sonochemistry, produce a dense unstructured cloud of bubbles below the tip, increasing in size and density as the power is raised. Such transducers also generate strong acoustic currents, which may carry the bubbles far from the radiating surface. For larger diameter sonotrodes, the bubbles form conical structures (Moussatov et al., 2003a, b), which appear to be formed by filaments originating from the transducer when recorded with short-term exposures. The conical structure has been explained by the action of the primary Bjerknes force in a high-amplitude spatially attenuated traveling wave (Koch et al., 2004b). Other structures can be found in the report of Mettin (2005).

5.4.5 Bubble Sizes and Lifetimes

In all the above observation, the bubble sizes recorded (see Mettin et al., 1999a, for the method used) amount to a few micrometers or less, for driving amplitudes ranging from 100 to 300 kPa. This is consistent with the theory of shape instabilities, confirmed experimentally by single-bubble experiments (see Fig. 2.10). Other measurements by laser techniques (Burdin et al., 1999) lead to the same conclusion. This rules out the early picture of cavitation activity by resonant bubbles, and the bubble sizes are in fact confined in a range between sub-micronic nuclei and radii slightly above the Blake threshold radius. This reduction of the parameter space to explore is of fundamental importance for theoretical aspects.

This conclusion should, however, be tempered since, even in this narrow range, the behavior of bubbles can still vary noticeably. This is not only true for the response curves (see Fig. 2.4), but even more for quantities like maximum temperature or shockwave intensities, which explains qualitatively why different structures produce different chemical or mechanical effects. Recent calculations even show that the chemical composition of bubbles can drastically change for acoustic pressure changing from 180 kPa (jellyfishes) to 300 kPa (sonotrode cavitation) (Yasui et al., 2005).

Another conclusion drawn from the above observations is the relatively long lifetime of bubbles in streamers and filaments (up to hundreds of cycles). This owes probably to the relatively low driving to which they are submitted. Such bubbles are excited above the Blake threshold, so that they are inertial and collapse at each cycle. Theory even predicts that they should grow by rectified diffusion up to the instability threshold (Louisnard and Gomez, 2003). The term “transient” would be used

improperly in this case, and this observation therefore constitutes a breakthrough in cavitation research.

There remain some uncertainties about the conversion of nuclei to inertial bubbles. In high-pressure zones, the nuclei could directly be excited above the Blake threshold. But in low-pressure zones, for example, at the starting point of streamers, how do the nuclei grow to an observable size? Competing effects of dissolution, migration toward pressure antinodes, and coalescence may give an answer, and a simplified theoretical study seems feasible.

5.5 How to Simulate Cavitation Fields

5.5.1 The Unknowns

Admitting that one could quantify the effect on a specific process (a chemical yield for example), of a bubble of ambient radius R_0 driven at a given acoustic pressure p_a, predicting a macroscopic effect requires knowledge of the spatial bubble distribution $N(\mathbf{x}, R_0)$. Observation of cavitation structures indicate that this quantity also varies with time, but on a timescale τ much larger than the acoustic period. The second unknown is the acoustic field itself $p_a(\mathbf{x}, t)$, exciting the various bubbles present at point $\mathbf{x}$.

Both quantities N and p_a are coupled (Leighton, 1995); the bubbles can drift under primary Bjerknes force, grow or dissolve, coalesce under secondary Bjerknes forces, or break up under the influence of the acoustic field. Conversely, the evolution of the bubble distribution in the liquid modifies the local sound velocity (see Equation (2.32)) and therefore the acoustic field.

5.5.2 Continuum Approach

Assuming that the bubble distribution is a continuous function $N(\mathbf{x}, \tau, R_0)$, of space $\mathbf{x}$, time τ, and bubble size R_0, its evolution can be described by a bubble conservation equation, sometimes referred as a population balance equation. In generic form, this equation can be written as

$$\frac{\partial N}{\partial \tau} + \nabla.(N\mathbf{v}) + \frac{\partial}{\partial R_0}(Nw) = B - D \tag{2.42}$$

where $\mathbf{v}$ is the bubble velocity, w the growth or dissolution rate, B the birth rate and D the death rate. Such equations are commonly used in crystallization. It must be emphasized that all terms must be based on the relevant physics, part of which has been given in this chapter. With an optimistic point of view $\mathbf{v}$ could be obtained from a balance of forces, and w from rectified diffusion theory. The birth term B arises from bubble nucleation, coalescence, and fragmentation, while D originates from the two latter processes, which are poorly documented. Mathematical difficulty moreover arises because of coalescence, which renders Equation (2.42)

integro-differential. The most complete equation relevant to cavitation can be found in Alekseev and Yushin (1986), but no solution was sought.

Among the various early attempts to obtain practical results from this equation, we mention the work of Kobelev and Ostrovskii (1983, 1989), who considered coalescence under secondary Bjerknes forces and bubble drift under primary ones, to interpret the self-illumination effect of sound observed in bubbly liquids (Kobelev et al., 1979). However these studies are limited to moderate sound fields, well below the Blake threshold.

More recently, in order to explain why experimentally observed bubble fields are always spatially inhomogeneous, Akhatov et al. (1994, 1996) demonstrated the spontaneous emergence of a bubble spatial distribution instability. They used an equation similar to Equation (2.42), accounting for bubble drift under Bjerknes forces and heuristic birth and death terms, coupled with a linear propagation equation in bubbly liquids. Finally, in order to assess the importance of coalescence on the bubble field formation, attempts were made to study the competition between coalescence and dissolution of bubbles under the Blake threshold (Louisnard, O. (2001). *Theoretical Study of Competition Between Dissolution and Coalescence of Small Bubbles in an Acoustic Field*, "Unpublished").

5.5.3 Particle Models

The continuum approach is of limited practical interest, especially to explain the formation of bubble streamers and filaments. Moreover, the inversion of Bjerknes forces needs non-linear bubble dynamics. Lauterborn and co-workers treated the individual bubbles as particles moving under the action of the forces, as described in Section 5.3 (Lauterborn et al., 1999; Mettin et al., 1999b; Parlitz et al., 1999). The standing acoustic wave is assumed undisturbed by the bubble motion and a monodisperse bubble ambient radius is assumed. Structures obtained by simulation with up to thousands of bubbles show outstanding similarities with several experimental filamentary structures (see the comparison in Fig. 2.12).

The assumption of a fixed standing wave was recently released by Mettin et al. (2006) by coupling the particle model to the propagation equation in bubbly liquids. The results predict the intermittency of both the filamentary bubble structure and the acoustic field, as experimentally observed. As far as we know, this is the most sophisticated model of cavitation fields, trapping the essential physics involved.

6 Final Remarks

6.1 Topics Not Addressed

The recent experimental observations reported in this chapter have been obtained at low-frequency cavitation, say, below 100 kHz. High-frequency cavitation is less documented experimentally (we refer the reader to recent high-speed photography observations by Chen et al., 2006, 2007). First, SBSL is only possible at low

frequencies, so that the high-frequency range did not benefit from this precious opportunity to observe and measure a single bubble. The theoretical results presented above should, however, also be relevant for high frequency. Three major differences with low frequency should be mentioned. First, the resonance radius is much lower (3 μm at 1 MHz), and thus very near the Blake critical radius. This suggests that bubbles at high frequency might approach the resonance radius more closely than they do at low frequencies. Second, the wavelength is much smaller at high frequency (1.5 mm at 1 MHz in water), which necessarily has implications on the bubble structures. For example, streamers that build between nodes and antinodes would be much smaller. The third difference has already been mentioned: the expansion phase is shorter at high frequency, which reduces the collapse strength.

Chopped ultrasound also constitutes an interesting issue. From a fundamental point of view, their study would shed light on the mechanisms of bubble population build-up. For example, it has been observed that the delay for the bubble cloud establishment depends in a non-monotonic way on the chopping mode (Labouret et al., 2006). Besides, in view of industrial applications, chopped ultrasound could reduce energy consumption noticeably.

Finally, for information on principles, design, and available types of ultrasonic transducers, we refer the reader to the articles of Gallego-Juarez (1999) and Mason (1999).

6.2 Further Readings

There is abundant literature on acoustic cavitation. The first comprehensive report on the subject dates back to Flynn (1964), who influenced generations of researchers on the topic. The physics of high-intensity fields (not only cavitation, but also absorption, radiation pressure, and acoustic streaming) can be found in Rozenberg (1971a). A wide collection of ultrasound applications is compiled in Rozenberg (1973). Plesset and Prosperetti (1977) proposed a review of early results on bubble dynamics. Many interesting references to early experimental work can be found in the report of Neppiras (1980). Leighton (1994) presents a sound approach of cavitation physics and a wide collection of references. A large collection of results on cavitation and diphasic flows can be found in Brennen (1995). The proceedings of the 1997 NATO conference on sonochemistry and sonoluminescence include an interesting collection of articles on both topics (Crum et al., 1999). The comprehensive theoretical and experimental work of Lauterborn's group is reviewed in Lauterborn et al. (1999). More recent observations by the same group can be found in Mettin (2005) and references herein.

For an early review of MBSL, we refer the reader to Walton and Reynolds (1984). SBSL literature is interesting not only for the phenomenon itself, but also because its interpretation covers a large part of cavitation physics. The review of Brenner et al. (2002) presents a fascinating historical overview on sonoluminescence (including

MBSL), a comprehensive presentation of single-bubble physics and a wide collection of references. Other interesting reviews on SBSL have been written by Hammer and Frommhold (2001) and Putterman and Weninger (2000).

Notations

a_n	amplitude of the nth-order spherical harmonic
b	damping coefficient for linear oscillations
B	birth rate of bubbles
c_l	sound speed in the liquid
C_∞	dissolved gas concentration far from the bubble
C_0	dissolved gas concentration at saturation $= p_0/k_g$
C_{p_g}	specific heat of the gas
C_{p_l}	specific heat of the liquid
C_R	dissolved gas concentration at the bubble wall $= p_g/k_g$
c.c.	conjugated complex number
c	effective sound speed in a bubbly liquid
D	death rate of bubbles
f	acoustic frequency $= \omega/2\pi$
$\mathbf{F}_\mathrm{A}$	buoyancy force
$\mathbf{F}_\mathrm{G}$	bubble weight
$\mathbf{F}_\mathrm{v}$	viscous drag force
$\mathbf{F}_\mathrm{M}$	added mass force
$\mathbf{F}_{\mathbf{B_1}}$	primary Bjerknes force
$\mathbf{F}_{\mathbf{B_2}}$	secondary Bjerknes force
$\mathbf{g}$	gravity
k_g	Henry's constant
K_g	thermal conductivity of the gas
K_l	thermal conductivity of the liquid
k_l	wavenumber of acoustic waves in the liquid
k	wavenumber of acoustic waves in the bubbly liquid
m_g	mass of incondensable gas in the bubble
M_g	molar mass of the incondensable gas in the bubble
$\mathbf{n}$	outward unit vector
N	bubble-size-distribution function
P	complex amplitude of the driving pressure
p_0	ambient pressure
$p(t), p(\mathbf{x}, t)$	driving pressure
p_a	depression in the liquid (for the quiet bubble)
p_a	amplitude of the driving (for single oscillating bubble)
$p_\mathrm{a}(\mathbf{x})$	complex amplitude of acoustic pressure
p_b	pressure in the bubble $= p_\mathrm{g} + p_\mathrm{v}$
p_g	gas partial pressure in the bubble

p_{g_0}	gas partial pressure in the bubble in ambient conditions
p_v	vapor partial pressure in the bubble
p_a^{crit}	Blake threshold
$p_{v,eq}$	vapor equilibrium saturation pressure
Pe	thermal Peclet number $= \tau_{diff}/\tau_{dyn}$
Pe_0	thermal Peclet number for linear oscillations
P_{active}	active acoustic power
P_{bound}	active acoustic power lost through boundaries
$\dot{Q}$	heat lost by the sonoreactor
r	local radius of a deformed bubble
R_0	ambient radius of the bubble
R	instantaneous radius of the bubble
R_i	radius at which the bubble interior starts to behave adiabatically
R_{min}	minimum bubble radius
R_{max}	maximum bubble radius
R_{res}	resonance radius
$\mathcal{R}$	universal gas constant
S	surface delimiting volume V
t	time
T	acoustic period
T_0	ambient temperature
T_C	bubble center temperature
T_R	bubble surface temperature
$\mathbf{u}$, u	liquid velocity
$\mathbf{u_a}$, u_a	complex amplitude of liquid velocity, in linear acoustics
U	internal energy of a volume of liquid
$\mathbf{v}$, v	bubble velocity
V	volume of liquid
V_1, V_2	instantaneous volumes of bubbles 1 and 2
w	growth or dissolution rate of the bubble
$\mathbf{x}$	spatial position
$\mathbf{x}_1$, $\mathbf{x}_2$	spatial positions of the centers of bubbles 1 and 2
X	complex amplitude of the bubble radius
Y_n	spherical harmonics
α_S	dimensionless Laplace tension $2\sigma/p_0R_0$
α	attenuation coefficient of linear wave
η	polytropic exponent
γ	ratio of the gas-specific heats
λ	wavelength
μ_l	dynamic viscosity of the liquid
Φ	complex number for thermal effects in the linear theory
ρ_l	liquid density
ρ_g	gas density
ρ_b	bubble density
σ	surface tension

τ_{dyn}	characteristic time of bubble oscillations
τ_{diff}	characteristic time of thermal diffusion
χ_{g}	thermal diffusivity of the gas
ω	angular frequency of the driving
ω_0	free angular frequency of the bubble

Subscripts

b refers to the bubble interior
g refers to the gas
l refers to the liquid
v refers to vapor

References

Akhatov, I., Gumerov, N., Ohl, C. D., Parlitz, U., and Lauterborn, W. (1997a). The role of surface tension in stable single bubble sonoluminescence. *Physics Review Letters*, 78(2), 227–230.

Akhatov, I., Mettin, R., Ohl, C. D., Parlitz, U., and Lauterborn, W. (1997b). Bjerknes force threshold for stable single bubble sonoluminescence. *Physical Review E*, 55(3), 3747–3750.

Akhatov, I., Parlitz, U., and Lauterborn, W. (1994). Pattern formation in acoustic cavitation. *Journal of the Acoustical Society of America*, 96(6), 3627–3635.

Akhatov, I., Parlitz, U., and Lauterborn, W. (1996). Towards a theory of self-organization phenomena in bubble-liquid mixtures. *Physical Review E*, 54(5), 4990–5003.

Alekseev, V. N., and Yushin, V. P. (1986). Distribution of bubbles in acoustic cavitation. *Soviet Physics Acoustics*, 32(6), 469–472.

Apfel, R. E. (1984). Acoustic cavitation inception. *Ultrasonics*, 22, 167–173.

Ashokkumar, M., Crum, L. A., Frensley, C. A., Grieser, F., Matula, T. J., McNamara, W. B., and Suslick, K. (2000). Effects of solutes on single-bubble sonoluminescence. *Journal of Physical Chemistry A*, 104, 8462–8465.

Ashokkumar, M., Guan, J., Tronson, R., Matula, T. J., Nuske, J. W., and Grieser, F. (2002). Effects of surfactants, polymers, and alcohols on single bubble dynamics and sonoluminescence. *Physical Review E*, 65, 046310–1–046310–4.

Augsdorfer, U. H., Evans, A. K., and Oxley, D. P. (2000). Thermal noise and the stability of single sonoluminescing bubbles. *Physical Review E*, 61(5), 5278–5285.

Barber, B. P., Hiller, R. A., Löfstedt, R., Putterman, S. J., and Weninger, K. R. (1997). Defining the unknowns of sonoluminescence. *Physics Report*, 281, 65–143.

Barber, B. P., Weninger, K. R., Putterman, S. J., and Löfstedt, R. (1995). Observation of a new phase of sonoluminescence at low partial pressures. *Physics Review Letters*, 74, 5276–5279.

Barber, B. P., Wu, C. C., Löfstedt, R., Roberts, P. H., and Putterman, S. J. (1994). Sensitivity of sonoluminescence to experimental parameters. *Physics Review Letters*, 72(9), 1380–1383.

Benjamin, T. B. (1958). Pressure waves from collapsing cavities. *2nd Symposium on Naval Hydrodynamics*, pp. 207–229, Washington.

Benjamin, T. B., and Ellis, A. T. (1966). The collapse of cavitation bubbles and the pressures thereby produced against solid boundaries. *Philosophical Transactions of the Royal Society London A*, 260(110), 221–240.

Benjamin, T. B., and Ellis, A. T. (1990). Self-propulsion of asymmetrically vibrating bubbles. *Journal of Fluid Mechanics*, 212(2), 65–80.

Blake, F. G. (1949). *The onset of cavitation in liquids; Technical memo 12*. Acoustic Research Laboratory, Cambridge, MA, Harvard University.

Blake, J. R., and Gibson, D. C. (1987). Cavitation bubbles near boundaries. *Annual Review of Fluid Mechanics*, 19, 99–123.

Brennen, C. E. (1995). *Cavitation and bubble dynamics*. Oxford Engineering Science Series, no. 44. New York, Oxford, Oxford University Press.

Brenner, M. P., Hilgenfeldt, S., and Lohse, D. (2002). Single-bubble sonoluminescence. *Reviews of Modern Physics*, 74(2), 425–483.

Brenner, M. P., Lohse, D., and Dupont, T. F. (1995). Bubble shape oscillations and the onset of sonoluminescence. *Physics Review Letters*, 75(5), 954–957.

Briggs, L. J. (1950). Limiting negative pressure of water. *Journal of Applied Physics*, 21, 721–722.

Burdin, F., Tsochatzidis, N. A., Guiraud, P., Wilhelm, A. M., and Delmas, H. (1999). Characterisation of the acoustic cavitation cloud by two laser techniques. *Ultrasonics Sonochemistry*, 6, 43–51.

Caflish, R. E., Miksis, M. J., Papanicolaou, G. C., and Ting, L. (1985). Effective equations for wave propagation in bubbly liquids. *Journal of Fluid Mechanics*, 153, 259–273.

Carstensen, E. L., and Foldy, L. L. (1947). Propagation of sound through a liquid containing bubbles. *Journal of the Acoustical Society of America*, 19(3), 481–501.

Chen, H., Li, X., and Wan, M. (2006). Spatial-temporal dynamics of cavitation bubble clouds in 1.2 MHz focused ultrasound field. *Ultrasonics Sonochemistry*, 13, 480–486.

Chen, H., Li, X., Wan, M., and Wang, S. (2007). High-speed observation of cavitation bubble cloud structures in the focal region of a 1.2 MHz high-intensity focused ultrasound transducer. *Ultrasonics Sonochemistry*, 14, 291–297.

Church, C. C. (1988). Prediction of rectified diffusion during nonlinear bubble pulsations at biomedical frequencies. *Journal of the Acoustical Society of America*, 83(6), 2210–2217.

Commander, K. W., and Prosperetti, A. (1989). Linear pressure waves in bubbly liquids: comparison between theory and experiments. *Journal of the Acoustical Society of America*, 85(2), 732–746.

Crum, L. A. (1975). Bjerknes forces on bubbles in a stationary sound field. *Journal of the Acoustical Society of America*, 57(6), 1363–1370.

Crum, L. A. (1980). Measurements of the growth of air bubbles by rectified diffusion. *Journal of the Acoustical Society of America*, 68(1), 203–211.

Crum, L. A. (1982). Nucleation and stabilization of microbubbles in liquids. *Applied Science Research*, 38(3), 101–115.

Crum, L. A. (1983). The polytropic exponent of gas contained within air bubbles pulsating in a liquid. *Journal of the Acoustical Society of America*, 73(1), 116–120.

Crum, L. A., and Eller, A. I. (1970). Motion of bubbles in a stationary sound field. *Journal of the Acoustical Society of America*, 48(1), 181–189.

Crum, L. A., and Hansen, G. M. (1982). Generalized equations for rectified diffusion. *Journal of the Acoustical Society of America*, 72(5), 1586–1592.

Crum, L. A., Mason, T. J., Reisse, J. L., and Suslick, K. S. (eds.). (1999). *Sonochemistry and Sonoluminescence*. Dordrecht, Kluwer. *Proceedings of the NATO Advanced Study Institute on Sonoluminescence and Sonoluminescence*, Leavenworth, Washington, DC, 18–29 August 1997.

Crum, L. A., and Prosperetti, A. (1983). Nonlinear oscillations of gas bubbles in liquids: an interpretation of some experimental results. *Journal of the Acoustical Society of America*, 73(1), 121–127.

Crum, L. A., and Prosperetti, A. (1984). Erratum and comments on "Nonlinear oscillations of gas bubbles in liquids: An interpretation of some experimental results". *Journal of the Acoustical Society of America – Letters to the Editor*, 75(6), 1910–1912.

Dähnke, S., Swamy, K. M., and Keil, F. J. (1999). Modeling of three-dimensional pressure fields in sonochemical reactors with an inhomogeneous density distribution of cavitation bubbles. Comparison of theoretical and experimental results. *Ultrasonics Sonochemistry*, 6, 31–41.

Devin, C. Jr. (1959). Survey of thermal, radiation and viscous damping of pulsating air bubbles in water. *Journal of the Acoustical Society of America*, 31(12), 1654–1667.

Didenko, Y. T., McNamara, W. B., and Suslick, K. S. (2000). Effect of noble gases on sonoluminescence temperatures during multibubble cavitation. *Physics Review Letters*, 84(4), 777–780.

Doinikov, A. A. (2004). Translational motion of a bubble undergoing shape oscillations. *Journal of Fluid Mechanics*, 501, 1–24.

Eller, A. I. (1972). Bubble growth by rectified diffusion in an 11-kHz sound field. *Journal of the Acoustical Society of America*, 52, 1447–1449.

Eller, A. I., and Crum, L. A. (1970). Instability of the motion of a pulsating bubble in a sound field. *Journal of the Acoustical Society of America*, 47(3), 762–767.

Eller, A.I, and Flynn, H. G. (1965). Rectified diffusion during nonlinear pulsations of cavitation bubbles. *Journal of the Acoustical Society of America*, 37, 493–503.

Epstein, P. S., and Plesset, M. S. (1950). On the stability of gas bubbles in liquid-gas solutions. *Journal of Chemical Physics*, 18, 1505–1509.

Flannigan, D. J., and Suslick, K. S. (2005). Plasma formation and temperature measurement during single-bubble cavitation. *Nature*, 434, 52–55.

Flint, E. B., and Suslick, K. S. (1991). The temperature of cavitation. *Science*, 253, 1397–1399.

Flynn, H. G. (1964). Physics of acoustic cavitation in liquids. In: Mason, W. P. (ed.), *Physical Acoustics*, vol. 1B, pp. 57–172. New York, NY, Academic.

Foldy, L. L. (1944). The multiple scattering of waves. *Physical Review*, 67(3–4), 107–119.

Fox, F. E., Curley, S. R., and Larson, G. S. (1955). Phase velocity and absorption measurements in water containing air bubbles. *Journal of the Acoustical Society of America*, 27(3), 534–539.

Fujikawa, S., and Akamatsu, T. (1980). Effects of the nonequilibrium condensation of vapour on the pressure wave produced by the collapse of a bubble in a liquid. *Journal of Fluid Mechanics*, 97, 481–512.

Fyrillas, M. M., and Szeri, A. J. (1994). Dissolution or growth of soluble spherical oscillating bubbles. *Journal of Fluid Mechanics*, 277, 381–407.

Fyrillas, M. M., and Szeri, A. J. (1995). Dissolution or growth of soluble spherical oscillating bubbles: the effect of surfactants. *Journal of Fluid Mechanics*, 289, 295–314.

Fyrillas, M. M., and Szeri, A. J. (1996). Surfactant dynamics and rectified diffusion of microbubbles. *Journal of Fluid Mechanics*, 311, 361–378.

Gaete-Garreton, L., Vargas-Hernandez, Y., Vargas-Herrera, R., Gallego-Juarez, J. A., and Montoya-Vitini, F. (1997). On the onset of cavitation in gassy liquids. *Journal of the Acoustical Society of America*, 101(5), 2536–2540.

Gaitan, D. F., and Holt, R. G. (1999). Experimental observations of bubble response and light intensity near the threshold for single bubble sonoluminescence in an air-water system. *Physical Review E*, 59, 5495–5502.

Gaitan, D. F., Crum, L. A., Church, C. C., and Roy, R. A. (1992). Sonoluminescence and bubble dynamics for a single, stable, cavitation bubble. *Journal of the Acoustical Society of America*, 91(6), 3166–3183.

Gallego-Juarez, J. A. (1999). High power ultrasonic transducers. In Crum, L. A., Mason, T. J., Reisse, J. L., and Suslick, K. S. (eds.), *Sonochemistry and sonoluminescence*. Dordrecht, Kluwer, pp. 259–270. *Proceedings of the NATO Advanced Study Institute on Sonoluminescence and Sonoluminescence*, Leavenworth, Washington, DC, 18–29 August 1997.

Goldman, D. E., and Ringo, G. R. (1949). Determination of pressure nodes in liquids. *Journal of the Acoustical Society of America*, 21, 270.

Gould, R. K. (1974). Rectified diffusion in the presence of, and absence of, acoustic streaming. *Journal of the Acoustical Society of America*, 56, 1740–1746.

Hammer, D., and Frommhold, L. (2000). Spectra of sonoluminescent rare-gas bubbles. *Physics Review Letters*, 85(6), 1326–1329.

Hammer, D., and Frommhold, L. (2001). Sonoluminescence: how bubbles glow. *Journal of Modern Optics*, 48, 239–277.

Hilgenfeldt, S., Brenner, M. P., Grossman, S., and Lohse, D. (1998). Analysis of Rayleigh-Plesset dynamics for sonoluminescing bubbles. *Journal of Fluid Mechanics*, 365, 171–204.

Hilgenfeldt, S., Grossmann, S., and Lohse, D. (1999a). A simple explanation of light emission in sonoluminescence. *Nature*, 398, 402–405.

Hilgenfeldt, S., Grossmann, S., and Lohse, D. (1999b). Sonoluminescence light emission. *Physics of Fluids*, 11, 1318–1330.

Hilgenfeldt, S., Lohse, D., and Brenner, M. P. (1996). Phase diagrams for sonoluminescing bubbles. *Physics of Fluids*, 8(11), 2808–2826.

Hiller, R. A., Putterman, S. J., and Barber, B. P. (1992). Spectrum of synchronous picosecond sonoluminescence. *Physics Review Letters*, 69(8), 1182–1184.

Hopkins, S. D., Putterman, S. J., Kappus, B. A., Suslick, K. S., and Camara, C. G. (2005). Dynamics of a sonoluminescing bubble in sulfuric acid. *Physics Review Letters*, 95(254301), 1–4.

Hsieh, D. Y., and Plesset, M. S. (1961). Theory of rectified diffusion of mass into gas bubbles. *Journal of the Acoustical Society of America*, 33, 206–215.

Iordansky, S. (1960). On the equations of motion for liquids containing gas bubbles. *Journal of Applied Mechancis and Technical Physics*, 3, 102–110.

Kamath, V., Oguz, H. N., and Prosperetti, A. (1992). Bubble oscillations in the nearly adiabatic limit. *Journal of the Acoustical Society of America*, 92(4), 2016–2023.

Kamath, V., and Prosperetti, A. (1989). Numerical integration methods in gas-bubble dynamics. *Journal of the Acoustical Society of America*, 85(4), 1538–1548.

Kamath, V., Prosperetti, A., and Egolfopoulos, F. N. (1993). A theoretical study of sonoluminescence. *Journal of the Acoustical Society of America*, 94(1), 248–260.

Kapustina, O. A. (1973). Degassing of liquids. In: Rozenberg, L. D. (ed.), *Physical principles of ultrasonic TECHNOLOGY*. New York, NY, Plenum Press.

Keller, J. B., and Miksis, M. (1980). Bubble oscillations of large amplitude. *Journal of the Acoustical Society of America*, 68, 628–633.

Ketterling, J. A., and Apfel, R. E. (1998). Experimental validation of the dissociation hypothesis for single bubble sonoluminescence. *Physics Review Letters*, 81, 4991–4994.

Ketterling, J. A., and Apfel, R. E. (2000). Extensive experimental mapping of sonoluminescence parameter space. *Physical Review E*, 61(4), 3832–3837.

Kobelev, Yu. A., and Ostrovskii, L. A. (1983). Collective self-effect of sound in a liquid with gas bubbles. *Journal of Experimental and Theoretical Physics Letters*, 37(1), 4–7.

Kobelev, Yu. A., and Ostrovskii, L. A. (1989). Nonlinear acoustic phenomena due to bubble drift in a gas-liquid mixture. *Journal of the Acoustical Society of America*, 85(2), 621–629.

Kobelev, Yu. A., Ostrovskii, L. A., and Sutin, A. M. (1979). Self-illumination effect for acoustic waves in a liquid with gas bubbles. *JETP Letters*, 30(7), 395–398.

Koch, P., Krefting, D., Tervo, T., Mettin, R., and Lauterborn, W. (2004a). Bubble path simulations in standing and traveling acoustic waves. *Proceedings of ICA 2004, Kyoto (Japan)*, vol. Fr3.A.2, pp. V3571–V3572.

Koch, P., Mettin, R., and Lauterborn, W. (2004b). Simulation of cavitation bubbles in travelling acoustic waves. In: Casseraeu, D. (ed.), *Proceedings CFA/DAGA04 Strasbourg, DEGA Oldenburg*, pp. 919–920.

Kornfeld, M., and Suvorov, L. (1944). On the destructive action of cavitation. *Journal of Applied Physics*, 15, 495–506.

Krefting, D., Mettin, R., and Lauterborn, W. (2004). High-speed observation of acoustic cavitation erosion in multibubble systems. *Ultrasonics Sonochemistry*, 11, 119–123.

Labouret, S., Frohly, J., and Rivart, F. (2006). Evolution of an 1 MHz ultrasonic cavitation bubble field in a chopped irradiation mode. *Ultrasonics Sonochemistry*, 13(4), 287–294.

Lauterborn, W. (1976). Numerical investigation of nonlinear oscillations of gas bubbles in liquids. *Journal of the Acoustical Society of America*, 59(2), 283–296.

Lauterborn, W., and Bolle, H. (1975). Experimental investigations of cavitation-bubble collapse in the neighborhood of a solid boundary. *Journal of Fluid Mechanics*, 72, 391–399.

Lauterborn, W., and Cramer, E. (1981a). On the dynamics of acoustic cavitation noise spectra. *Acustica*, 49, 280–287.

Lauterborn, W., and Cramer, E. (1981b). Subharmonic route to chaos observed in acoustics. *Physics Review Letters*, 47(20), 1445–1448.

Lauterborn, W., Kurz, T., Mettin, R., and Ohl, C. D. (1999). Experimental and theoretical bubble dynamics. *Advanced in Chemical Physics*, 110, 295–380.

Lauterborn, W., and Mettin, R. (1999). Nonlinear bubble dynamics: response curves and more. In: Crum, L. A., Mason, T. J., Reisse, J. L., and Suslick, K. S. (eds.), *Sonochemistry and Sonoluminescence*, pp. 63–72. Dordrecht, Kluwer. *Proceedings of the NATO Advanced Study Institute on Sonoluminescence and Sonoluminescence*, Leavenworth, Washington, DC, 18–29 August 1997.

Leighton, T. G. (1994). *The acoustic bubble*. London, Academic.

Leighton, T. G. (1995). Bubble population phenomena in acoustic cavitation. *Ultrasonics Sonochemistry*, 2(2), S123–S136.

Lezzi, A., and Prosperetti, A. (1987). Bubble dynamics in a compressible liquid. Part 2. Second-order theory. *Journal of Fluid Mechanics*, 185, 289–321.

Li, M. K., and Fogler, H. S. (2004). Acoustic emulsification. Part 2. Breakup of the large primary oil droplets in a water medium. *Journal of Fluid Mechanics*, 88, 513–528.

Lin, H., Storey, B. D., and Szeri, A. J. (2002a). Inertially driven inhomogeneities in violently collapsing bubbles: the validity of the Rayleigh-Plesset equation. *Journal of Fluid Mechanics*, 452(10), 145–162.

Lin, H., Storey, B. D., and Szeri, A. J. (2002b). Rayleigh-Taylor instability of violently collapsing bubbles. *Physics of Fluids*, 14(8), 2925–2928.

Lindau, O., and Lauterborn, W. (2003). Cinematographic observation of the collapse and rebound of a laser-produced cavitation bubble near a wall. *Journal of Fluid Mechanics*, 479, 327–348.

Löfstedt, R., Barber, B. P., and Putterman, S. J. (1993). Toward a hydrodynamic theory of sonoluminescence. *Physics of Fluids*, A5(11), 2911–2928.

Löfstedt, R., Weninger, K., Putterman, S., and Barber, B. P. (1995). Sonoluminescing bubbles and mass diffusion. *Physical Review E*, 51(5), 4400–4410.

Lohse, D., and Hilgenfeldt, S. (1997). Inert gas accumulation in sonoluminescing bubbles. *Journal of Chemical Physics*, 107(17), 6986–6997.

Lohse, D., Brenner, M. P., Dupont, T. F., Hilgenfeldt, S., and Johnston, B. (1997). Sonoluminescing air bubbles rectify argon. *Physics Review Letters*, 78(7), 1359–1362.

Louisnard, O., and Gomez, F. (2003). Growth by rectified diffusion of strongly acoustically forced gas bubbles in nearly saturated liquids. *Physical Review E*, 67(036610), 1–12.

Magnaudet, J. (1997). The forces acting on bubbles and rigid particles. In: *ASME Fluids Engineering Division Summer Meeting*, Vancouver, Canada, paper 97–3522.

Magnaudet, J., and Legendre, D. (1998). The viscous drag force on a spherical bubble with a time-dependent radius. *Physics of Fluids*, 10, 550–554.

Mason, T. J. (1999). Laboratory equipment and usage considerations. In: Crum, L. A., Mason, T. J., Reisse, J. L., and Suslick, K. S. (eds.), *Sonochemistry and sonoluminescence*, pp. 245–258. Dordrecht, Kluwer. *Proceedings of the NATO Advanced Study Institute on Sonoluminescence and Sonoluminescence*, Leavenworth, Washington, DC, 18–29 August 1997.

Matula, T. J. (2000). Single-bubble sonoluminescence in microgravity. *Ultrasonics*, 357, 203–223.

Matula, T. J., and Crum, L. A. (1998). Evidence of gas exchange in single-bubble sonoluminescence. *Physics Review Letters*, 80(4), 865–868.

Matula, T. J., Roy, R. A., Mourad, P. D., McNamara, W. B., and Suslick, K. S. (1995). Comparison of multibubble and single-bubble sonoluminescence spectra. *Physics Review Letters*, 75(13), 2602–2605.

McNamara, W. B., Didenko, Y. T., and Suslick, K. S. (1999). Sonoluminescence temperatures during multi-bubble cavitation. *Nature*, 401, 772–775.

Mettin, R. (2005). Bubble structures in acoustic cavitation. In: Doinikov, A. A. (ed.), *Bubble and particle dynamics in acoustic fields: Modern trends and applications*, pp. 1–36. Kerala (India), Research Signpost.

Mettin, R., Akhatov, I., Parlitz, U., Ohl, C. D., and Lauterborn, W. (1997). Bjerknes force between small cavitation bubbles in a strong acoustic field. *Physical Review E*, 56(3), 2924–2931.

Mettin, R., Koch, P., Lauterborn, W., and Krefting, D. (11-15 September 2006). Modeling acoustic cavitation with bubble redistribution. *Sixth International Symposium on Cavitation – CAV2006 (Paper 75)*, Wageningen (The Netherlands), pp. 125–129.

Mettin, R., Luther, S., and Lauterborn, W. (1999a). Bubble size distribution and structures in acoustic cavitation. *Proceedings of 2nd conference on Applications of Power Ultrasound in Physical and Chemical Processing*, Toulouse, France, pp. 125–129.

Mettin, R., Luther, S., Ohl, C. D., and Lauterborn, W. (1999b). Acoustic cavitation structures and simulations by a particle model. *Ultrasonics Sonochemistry*, 6, 25–29.

Miksis, M. J., and Ting, L. (1984). Nonlinear radial oscillations of a gas bubble including thermal effects. *Journal of the Acoustical Society of America*, 76(3), 897–905.

Moussatov, A., Granger, C., and Dubus, B. (2003a). Cone-like bubble formation in ultrasonic cavitation field. *Ultrasonics Sonochemistry*, 10, 191–195.

Moussatov, A., Mettin, R., Granger, C., Tervo, T., Dubus, B., and Lauterborn, W. (2003b, 7-10 September). Evolution of acoustic cavitation structures near larger emitting surface. *Proceedings of the World Congress on Ultrasonics*, Paris (France), pp. 955–958.

Neppiras, E. A. (1969). Subharmonic and other low-frequency emission from bubbles in sound-irradiated liquids. *Journal of the Acoustical Society of America*, 46, 587–601.

Neppiras, E. A. (1980). Acoustic cavitation. *Physics Report*, 61, 159–251.

Noltingk, B. E., and Neppiras, E. A. (1950). Cavitation produced by ultrasonics. *Proceedings of the Physical Society*, B63, 674–685.

Nyborg, W. L., and Hughes, D. E. (1967). Bubble annihilation in cavitation streamers. *Journal of the Acoustical Society of America*, 42(4), 891–894.

Oguz, H. N., and Prosperetti, A. (1990). A generalization of the impulse and virial theorems with an application to bubble oscillations. *Journal of Fluid Mechanics*, 218, 143–162.

Ohl, C. D., Lindau, O., and Lauterborn, W. (1998). Luminescence from spherically and aspherically collapsing laser bubbles. *Physics Review Letters*, 80, 393–396.

Parlitz, U., Mettin, R., Luther, S., Akhatov, I., Voss, M., and Lauterborn, W. (1999). Spatio temporal dynamics of acoustic cavitation bubble clouds. *Philosophical Transactions of the Royal Society London A*, 357, 313–334.

Pecha, R., and Gompf, B. (2000). Microimplosions: cavitation collapse and shock wave emission on a nanosecond time scale. *Physics Review Letters*, 84(6), 1328–1330.

Pelekasis, N. A., and Tsamopoulos, J. A. (1993). Bjerknes forces between two bubbles. Part 2. Response to an oscillatory pressure field. *Journal of Fluid Mechanics*, 254, 501–527.

Pétrier, C., and Francony, A. (1997). Ultrasonic waste-water treatment: incidence of ultrasonic frequency on the rate of phenol and carbon tetrachloride degradation. *Ultrasonics Sonochemistry*, 4, 295–300.

Philipp, A., and Lauterborn, W. (1998). Cavitation erosion by single laser-produced bubbles. *Journal of Fluid Mechanics*, 361, 75–116.

Plesset, M. S. (1949). The dynamics of cavitation bubbles. *Journal of Applied Mechanics*, 16, 277–282.

Plesset, M. S., and Mitchell, T. P. (1956). On the stability of the spherical shape of a vapor cavity in a liquid. *Quarterly of Applied Mathematics*, 13(4), 419–430.

Plesset, M. S., and Prosperetti, A. (1977). Bubble dynamics and cavitation. *Annual Review of Fluid Mechanics*, 9, 145–185.

Prosperetti, A. (1977a). Thermal effects and damping mechanisms in the forced radial oscillations of gas bubbles in liquids. *Journal of the Acoustical Society of America*, 61(1), 17–27.

Prosperetti, A. (1977b). Viscous effects on perturbed spherical flows. *Quarterly of Applied Mathematics*, 34, 339–352.

Prosperetti, A. (1991). The thermal behaviour of oscillating gas bubbles. *Journal of Fluid Mechanics*, 222, 587–616.

Prosperetti, A. (1997). A new mechanism for sonoluminescence. *Journal of the Acoustical Society of America*, 101(4), 2003–2007.

Prosperetti, A. (1999). Old-fashioned bubble dynamics. In: Crum, L. A., Mason, T. J., Reisse, J. L., and Suslick, K. S. (eds.), *Sonochemistry and sonoluminescence*, pp. 39–62. Dordrecht, Kluwer. *Proceedings of the NATO Advanced Study Institute on Sonoluminescence and Sonoluminescence*, Leavenworth, Washington, DC, 18–29 August 1997.

Prosperetti, A., and Hao, Y. (1999). Modelling of spherical gas bubble oscillations and sonoluminescence. *Philosophical Transactions of the Royal Society London A*, 357, 203–223.

Prosperetti, A., and Lezzi, A. (1986). Bubble dynamics in a compressible liquid. Part 1. First-order theory. *Journal of Fluid Mechanics*, 168, 457–478.

Prosperetti, A., and Seminara, G. (1978). Linear stability of a growing or collapsing bubble in a slightly viscous liquid. *Physics of Fluids*, 21(9), 1465–1470.

Prosperetti, A., Crum, L. A., and Commander, K. W. (1988). Nonlinear bubble dynamics. *Journal of the Acoustical Society of America*, 83, 502–514.

Putterman, S. J., and Weninger, K. R. (2000). Sonoluminescence: How bubbles turn into light. *Annual Review of Fluid Mechanics*, 32, 445–476.

Ratoarinoro, Contamine, F., Wilhelm, A. M., Berlan, J., and Delmas, H. (1995). Power measurement in sonochemistry. *Ultrasonics Sonochemistry*, 2(1), S43–S47.

Rayleigh, Lord. (1917). On the pressure developed in a liquid during the collapse of a spherical cavity. *Philosophical Magazine*, 34, 94–98.

Reddy, A. J., and Szeri, A. J. (2002). Shape stability of unsteadily translating bubbles. *Physics of Fluids*, 14(7), 2216–2224.

Rozenberg, L. D. (ed.). (1971a). *High-intensity ultrasonic fields*. New York, NY, Plenum Press.

Rozenberg, L. D. (1971b). The cavitation zone. In: Rozenberg, L. D. (ed.), *High-intensity ultrasonic fields*. New-York, NY, Plenum Press.

Rozenberg, L. D. (ed.). (1973). *Physical principles of ultrasonic technology*. New York, NY, Plenum Press.

Servant, G., Caltagirone, J. P., Girard, A., Laborde, J. L., and Hita, A. (2000). Numerical simulation of cavitation bubble dynamics induced by ultrasound waves in a high frequency reactor. *Ultrasonics Sonochemistry*, 7, 217–227.

Servant, G., Laborde, J. L., Hita, A., Caltagirone, J. P., and Girard, A. (2003). On the interaction between ultrasound waves and bubble clouds in mono- and dual-frequency sonoreactors. *Ultrasonics Sonochemistry*, 10(6), 347–355.

Silberman, E. (1957). Sound velocity and attenuation in bubbly mixtures measured in standing wave tubes. *Journal of the Acoustical Society of America*, 29(8), 925–933.

Sirotyuk, M. G. (1971). Experimental investigations of ultrasonic cavitation. In: Rozenberg, L. D. (ed.), *High-intensity ultrasonic fields*. New-York, NY, Plenum Press.

Storey, B. D., and Szeri, A.J. (2000). Water vapour, sonoluminescence and sonochemistry. *Proceedings of the Royal Society of London, Series A*, 456, 1685–1709.

Storey, B. D., and Szeri, A.J. (2001). A reduced model of cavitation physics for use in sonochemistry. *Proceedings of the Royal Society of London, Series A*, 457, 1685–1700.

Storey, B. D., and Szeri, A. J. (2002). Argon rectification and the cause of light emission in single-bubble sonoluminescence. *Physics Review Letters*, 88(7), 074301-1–074301-3.

Storey, B. D., Lin, H., and Szeri, A. J. (2001). Physically realistic models of catastrophic bubble collapses. In: *Fourth International Symposium on Cavitation*. California Institute of Technology, Pasadena, CA, June 20–23.

Strasberg, A. (1961). Rectified diffusion: Comments on a paper of Hsieh and Plesset. *Journal of the Acoustical Society of America – Letters to the Editor*, 33, 359.

Strasberg, M., and Benjamin, T. B. (1958). Excitation of oscillations in the shape of pulsating gas bubbles. *Journal of the Acoustical Society of America (Abstract)*, 30, 697.

Suslick, K. S., McNamara, W. B., and Didenko, Y. (1999). Hot spot conditions during multi-bubble cavitation. In: Crum, L. A., Mason, T. J., Reisse, J. L., and Suslick, K. S. (eds.), *Sonochemistry and sonoluminescence*, pp. 191–204. Dordrecht, Kluwer. *Proceedings of the NATO Advanced Study Institute on Sonoluminescence and Sonoluminescence*, Leavenworth, Washington, DC, 18–29 August 1997.

Toegel, R., Gompf, B., Pecha, R., and Lohse, D. (2000a). Does water vapor prevent upscaling sonoluminescence? *Physics Review Letters*, 85(15), 3165–3168.

Toegel, R., Hilgenfeldt, S., and Lohse, D. (2000b). Squeezing alcohols into sonoluminescing bubbles: the universal role of surfactants. *Physics Review Letters*, 84(11), 2509–2512.

Tomita, Y., and Shima, A. (1977). On the behaviour of a spherical bubble and the impulse pressure in a viscous compressible liquid. *Bulletin of the JSME*, 20(149), 1453–1460.

Vazquez, G. E., and Putterman, S. J. (2000). Tempurature and pressure dependence of sonoluminescence. *Physics Review Letters*, 85(14), 3037–3040.

Walton, A. J., and Reynolds, G. T. (1984). Sonoluminescence. *Advances in Physics*, 33(6), 595–660.

Wijngaarden, V. L. (1968). On the equations of motion for mixtures of liquid and gas bubbles. *Journal of Fluid Mechanics*, 33(3), 465–474.

Yasui, K. (1997). Alternative model of single-bubble sonoluminescence. *Physical Review E*, 56, 6750–6760.

Yasui, K. (2001). Effect of liquid temperature on sonoluminescence. *Physical Review E*, 64(016310), 1–10.

Yasui, K., Tuziuti, T., and Iida, Y. (2005). Dependence of the characteristics of bubbles on types of sonochemical reactors. *Ultrasonics Sonochemistry*, 12, 43–51.

Yuan, L., Ho, C. Y., Chu, M. C., and Leung, P. T. (2001). Role of gas density in the stability of single-bubble sonoluminescence. *Physical Review E*, 64(016317), 1–6.

Zardi, D., and Seminara, G. (1995). Chaotic mode competition in the shape oscillations of pulsating bubbles. *Journal of Fluid Mechanics*, 286, 257–276.